







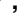











RESEARCH ARTICLE

Boosting subdominant neutralizing antibody responses with a computationally designed epitope-focused immunogen

Fabian Sesterhenn ^{1,2}, Marie Galloux ³, Sabrina S. Vollers ¹, Lucia Csepregi ⁴, Che Yang ^{1,2}, Delphine Descamps ³, Jaume Bonet ^{1,2}, Simon Friedensohn ⁴, Pablo Gainza ^{1,2}, Patricia Corthésy ¹, Man Chen ⁵, Stéphane Rosset ¹, Marie-Anne Rameix-Welti ^{6,7}, Jean-François Éléouët ³, Sai T. Reddy ⁴, Barney S. Graham ⁵, Sabine Riffault ³, Bruno E. Correia ^{1,2*}

1 Institute of Bioengineering, École Polytechnique Fédérale de Lausanne, Lausanne, Switzerland, **2** Swiss Institute of Bioinformatics (SIB), Lausanne, Switzerland, **3** Unité de Virologie et Immunologie Moléculaires (UR892), INRA, Université Paris-Saclay, Jouy-en-Josas, France, **4** Department of Biosystems Science and Engineering, ETH Zurich, Basel, Switzerland, **5** Viral Pathogenesis Laboratory, Vaccine Research Center, National Institute of Allergy and Infectious Diseases, National Institutes of Health, Bethesda, Maryland, United States of America, **6** UMR1173, INSERM, Université de Versailles St. Quentin, Montigny le Bretonneux, France, **7** AP-HP, Laboratoire de Microbiologie, Hôpital Ambroise Paré, Boulogne-Billancourt, France

* bruno.correia@epfl.ch


 OPEN ACCESS

Citation: Sesterhenn F, Galloux M, Vollers SS, Csepregi L, Yang C, Descamps D, et al. (2019) Boosting subdominant neutralizing antibody responses with a computationally designed epitope-focused immunogen. *PLoS Biol* 17(2): e3000164. <https://doi.org/10.1371/journal.pbio.3000164>

Academic Editor: James Munro, Tufts University, UNITED STATES

Received: November 16, 2018

Accepted: February 8, 2019

Published: February 21, 2019

Copyright: © 2019 Sesterhenn et al. This is an open access article distributed under the terms of the [Creative Commons Attribution License](https://creativecommons.org/licenses/by/4.0/), which permits unrestricted use, distribution, and reproduction in any medium, provided the original author and source are credited.

Data Availability Statement: Data supporting the findings of this study are available within the article and its Supporting Information or are available from the authors upon request. Next-generation sequencing data are available under NCBI BioProject number PRJNA515493.

Funding: FS was supported by the Swiss initiative for systems biology (SystemsX.ch). BEC was supported by the European Research Council (Starting grant - 716058) and the Swiss National

Abstract

Throughout the last several decades, vaccination has been key to prevent and eradicate infectious diseases. However, many pathogens (e.g., respiratory syncytial virus [RSV], influenza, dengue, and others) have resisted vaccine development efforts, largely because of the failure to induce potent antibody responses targeting conserved epitopes. Deep profiling of human B cells often reveals potent neutralizing antibodies that emerge from natural infection, but these specificities are generally subdominant (i.e., are present in low titers). A major challenge for next-generation vaccines is to overcome established immunodominance hierarchies and focus antibody responses on crucial neutralization epitopes. Here, we show that a computationally designed epitope-focused immunogen presenting a single RSV neutralization epitope elicits superior epitope-specific responses compared to the viral fusion protein. In addition, the epitope-focused immunogen efficiently boosts antibodies targeting the palivizumab epitope, resulting in enhanced neutralization. Overall, we show that epitope-focused immunogens can boost subdominant neutralizing antibody responses in vivo and reshape established antibody hierarchies.

Author summary

Vaccines are one of the most valuable instruments to prevent and control infectious diseases. Their primary correlate of protection is the level of induction of neutralizing antibodies that target critical antigenic sites and thereby block infection. Natural infections with pathogens such as the respiratory syncytial virus (RSV) or influenza induce a broad repertoire of antibodies that target multiple epitopes. Among those, functional antibodies

Science Foundation (Schweizerischer Nationalfonds zur Förderung der Wissenschaftlichen Forschung; 310030_163139). The funders had no role in study design, data collection and analysis, decision to publish, or preparation of the manuscript.

Competing interests: The authors have declared that no competing interests exist.

Abbreviations: bnAb, broadly neutralizing antibody; DLS, dynamic light scattering; ELISpot, enzyme-linked immunospot assay; HA, hemagglutinin; HCDR3, heavy chain complementarity-determining region 3; N.D., nondetectable; nAb, neutralizing antibody; NCBI, National Center for Biotechnology Information; NGS, next-generation antibody repertoire sequencing; NHP, nonhuman primate; PDB, Protein Data Bank; RLU, relative light units; RSV, respiratory syncytial virus; RSVF, RSV fusion protein; RSVN, RSV nucleoprotein; SPR, surface plasmon resonance.

with key specificities are often subdominant (present in low titers). Thus, a central goal for vaccine development is to focus antibody responses on such neutralization epitopes. Here, we show that a computationally designed, epitope-focused immunogen mimicking an important RSV neutralization epitope (site II) can focus antibodies onto this well-defined epitope. In a scenario of preexisting immunity, in which site II-specific antibodies were subdominant, the epitope-focused immunogen selectively boosted site II-specific antibodies, resulting in an increased viral neutralization through this epitope. We propose that rationally designed immunogens spotlighting defined epitopes have a unique potential to focus antibody responses on functionally conserved sites in cases of preexisting immunity. Our results have broad implications for vaccine design as a strategy to steer preexisting antibody responses away from immunodominant, variable epitopes and toward subdominant epitopes that confer broad and potent neutralization.

Introduction

The development of vaccines has proven to be one of the most successful medical interventions to reduce the burden of infectious diseases [1], and their correlate of protection is the induction of neutralizing antibodies (nAbs) that block infection [2].

In recent years, advances in high-throughput B cell technologies have revealed a plethora of potent nAbs for different pathogens that have resisted the traditional means of vaccine development for several decades, including HIV-1 [3], influenza [4], respiratory syncytial virus (RSV) [5, 6], Zika [7, 8], dengue [9], and others [10–12]. A major target of these nAb responses is the pathogen's fusion protein, which drives the viral and host cell membrane fusion while undergoing a conformational rearrangement from a prefusion to a postfusion state [13]. Many of these nAbs have been structurally characterized in complex with their target, unveiling the atomic details of neutralization epitopes [7, 14, 15]. Together, these studies have provided comprehensive antigenic maps of the viral fusion proteins, which delineate epitopes susceptible to antibody-mediated neutralization and provide a road map for rational and structure-based vaccine design approaches.

The conceptual framework to leverage nAb-defined epitopes for vaccine development is commonly referred to as reverse vaccinology [16–18]. Although reverse vaccinology-inspired approaches have yielded a number of exciting advances in the last decade, the design of immunogens that elicit such focused antibody responses remains challenging. Successful examples of structure-based immunogen design approaches include conformational stabilization of RSV fusion protein (RSVF) in its prefusion state, which induces superior serum neutralization titers when compared to immunization with RSVF in the postfusion conformation [19]. In the case of influenza, several epitopes targeted by broadly neutralizing antibodies (bnAbs) were identified within the hemagglutinin (HA) stem domain, and an HA stem-only immunogen elicited a broader nAb response than full-length HA [20, 21]. Commonly, these approaches have aimed to focus antibody responses on specific conformations or subdomains of viral proteins. In a more aggressive approach, Correia and colleagues [22] computationally designed a synthetic immunogen presenting the RSV antigenic site II and provided a proof of principle for the induction of site-specific, RSV nAbs, using a synthetic immunogen.

The absence of a potent and long-lasting immune response upon natural infection is a major challenge associated with RSV, influenza virus, and other pathogens. Whereas a single exposure to pathogens like poliovirus confers life-long immunity, RSV, influenza, and other pathogens have developed mechanisms to subvert the development of a durable and potent

nAb response, thereby allowing such pathogens to infect humans repeatedly throughout their lives [23]. One of the major factors hindering the induction of long-lasting protection after the first infection is related to the antibody specificities induced. Upon exposure to a pathogen, such as influenza, the human antibody responses predominantly target strain-specific antigenic sites, whereas potent bnAbs are subdominant [24]. This phenomenon is generally referred to as B cell immunodominance, which describes the unbalanced immunogenicity of certain antigenic sites within an antigen, favoring strain-specific, variable, nonneutralizing epitopes to the detriment of conserved, neutralization-sensitive epitopes [25]. The factors that determine the antigenicity of specific epitopes remain unclear, making the categorization of immunodominant and subdominant epitopes an empirical classification based on serological analysis. The presence of high levels of antibodies directed against immunodominant epitopes can sterically mask surrounding subdominant epitopes that may be targeted by bnAbs, preventing the immune system from mounting productive antibody responses against subdominant epitopes and potentially limiting vaccination efficacy [24–27].

The immunodominance hierarchy is established within the germinal center, where B cells undergo a binding affinity-based competition for available antigen and subsequently initiate a clonal expansion stage, ultimately becoming long-lived plasma cells or memory B cells [28]. Controlling this competition and driving antibody responses toward the increased recognition of subdominant, neutralizing epitopes is of primary importance to enable development of novel vaccines against pathogens that have resisted traditional strategies. One of the few strategies to guide antibody maturation was tested in the HIV field and is referred to as germline targeting, which relies upon the activation and expansion of rare but specific B cell lineages in naïve individuals [29, 30]. In contrast, under conditions of preexisting immunity acquired during natural infection or previous vaccination, the challenge is to manipulate already established B cell immunodominance hierarchies and reshape serum antibody responses toward desired specificities. In an indirect approach toward increasing subdominant B cell populations, Silva and colleagues [31] have shown that the targeted suppression of immunodominant clones during an active germinal center reaction can allow subdominant B cell populations to overtake the germinal center response. Other approaches have used heterologous prime–boost immunization regimens with either alternative viral strains or rationally modified versions of the priming immunogen in order to steer antibody responses toward more conserved domains [32–35]. However, leveraging structural information of defined neutralization epitopes to guide bulk antibody responses toward specific, well-characterized single epitopes remains an unmet challenge.

Here, we investigate whether, under conditions of preexisting immunity, a computationally designed immunogen presenting a single epitope is able to reshape serum antibody responses toward increased recognition of a specific neutralizing epitope. To mimic a scenario of preexisting immunity against a relevant pathogen, we immunized mice with a prefusion-stabilized version of RSVF and found that antibody titers against RSV antigenic site II were present in very low levels—i.e., a subdominant site II-specific response was elicited. Based on a previously developed epitope-focused immunogen for RSV site II (FFL_001) [22], we engineered an optimized nanoparticle presenting this immunogen and investigated the potential of a rationally designed epitope-focused immunogen to boost these subdominant levels of site-specific antibodies.

We show that multivalent presentation of a designed epitope-focused immunogen elicits superior levels of epitope-specific antibodies compared to prefusion RSVF in naïve mice, indicating that the subdominance of a particular epitope can be altered through its presentation in a distinct molecular context. Repeated immunizations with RSVF failed to increase site II-specific antibodies and instead further dampened site II-specific responses. In contrast, heterologous boosts with an epitope-scaffold nanoparticle enhanced serum responses toward the subdominant site II epitope, and the boosted antibodies neutralized RSV *in vitro*. For the first

time, to our knowledge, we provide compelling evidence that synthetic immunogens comprising a single epitope can efficiently redirect specificities in bulk antibody responses *in vivo* and enhance subdominant nAb responses. Such strategy may present an important alternative for pathogens in which future vaccines are required to reshape preexisting immunity and elicit finely tuned antibody specificities.

Results

Design of an RSV-based nanoparticle displaying a site II epitope-focused immunogen

In a previous study, a computationally designed, RSV site II epitope-scaffold nanoparticle was shown to elicit serum neutralization activity in nonhuman primates (NHPs) [22]. Despite the fact that very potent monoclonal antibodies were isolated from the immunized NHPs, the neutralization potency at the serum level was modest, indicating low titers of the potent antibodies. Therefore, our first aim was to take the best previously tested immunogen (FFL_001) and further optimize delivery and immunization conditions to maximize the induction of site II-specific antibodies. A comparative study of four different adjuvants revealed that alum, an adjuvant approved for human use, yielded the highest overall immunogenicity and elicited antibodies cross-reactive with prefusion RSVF in four out of five mice (S1 Fig).

Next, we sought to develop an improved, easily produced nanoparticle to multimerize the epitope-scaffold for efficient B cell receptor cross-linking. Previously, Correia and colleagues [22] employed a chemical conjugation strategy of FFL_001 to a hepatitis B core antigen-based nanoparticle, which resulted in a difficult construct with a laborious purification process. Recently, several studies have reported the use of the RSV nucleoprotein (RSVN) as a nanoparticle platform for immunogen presentation [36, 37]. When expressed in *Escherichia coli*, RSVN forms nanorings, 17 nm in diameter, containing 10 or 11 RSVN protomers [38]. We reasoned that RSVN would be an ideal particle platform to multimerize an RSV epitope-scaffold, as RSVN contains strong, RSV-directed T-cell epitopes [37]. However, our initial attempts to genetically fuse FFL_001 to RSVN yielded poorly soluble proteins that rapidly aggregated after purification. We therefore employed structure-based protein resurfacing [39], attempting to improve the solubility of this site II epitope-scaffold when arrayed in high density on RSVN. To guide our resurfacing design process, we leveraged information from a sequence homolog of the ribosomal recycling factor (Protein Data Bank [PDB]: 1ISE), the structural template originally used to design FFL_001. Based on a sequence alignment of the mouse homolog (National Center for Biotechnology Information [NCBI] reference: NP_080698.1) and FFL_001, we exchanged the FFL_001 amino acids for the mouse sequence homolog and used Rosetta fixed backbone design [40] to ensure that the mutations were not energetically unfavorable, resulting in 38 amino acid substitutions (34.2% overall). We named this variant FFLM, whose expression yields in *E. coli* showed a 5-fold increase when compared to FFL_001, and it was confirmed to be monomeric in solution (S2 Fig).

To confirm that the resurfacing did not alter the epitope integrity, we measured the binding affinities of FFLM to motavizumab, a high-affinity variant of palivizumab [41], and to a panel of human site II nAbs previously isolated [5], using surface plasmon resonance (SPR). All antibodies bound with high affinity to FFLM, indicating broad reactivity of this immunogen with a diverse panel of human nAbs (Figs 1B and S3). The tested nAbs showed approximately one order of magnitude higher affinity to the epitope-scaffold as compared to the latest version of prefusion RSVF, originally called DS2 [42], suggesting that the epitope is properly presented and likely further stabilized in a relevant conformation.

The FFLM-RSVN fusion protein expressed with high yields in *E. coli* (>10 mg/liter), forming a nanoring particle, dubbed NRM, that was monodisperse in solution, with a diameter of

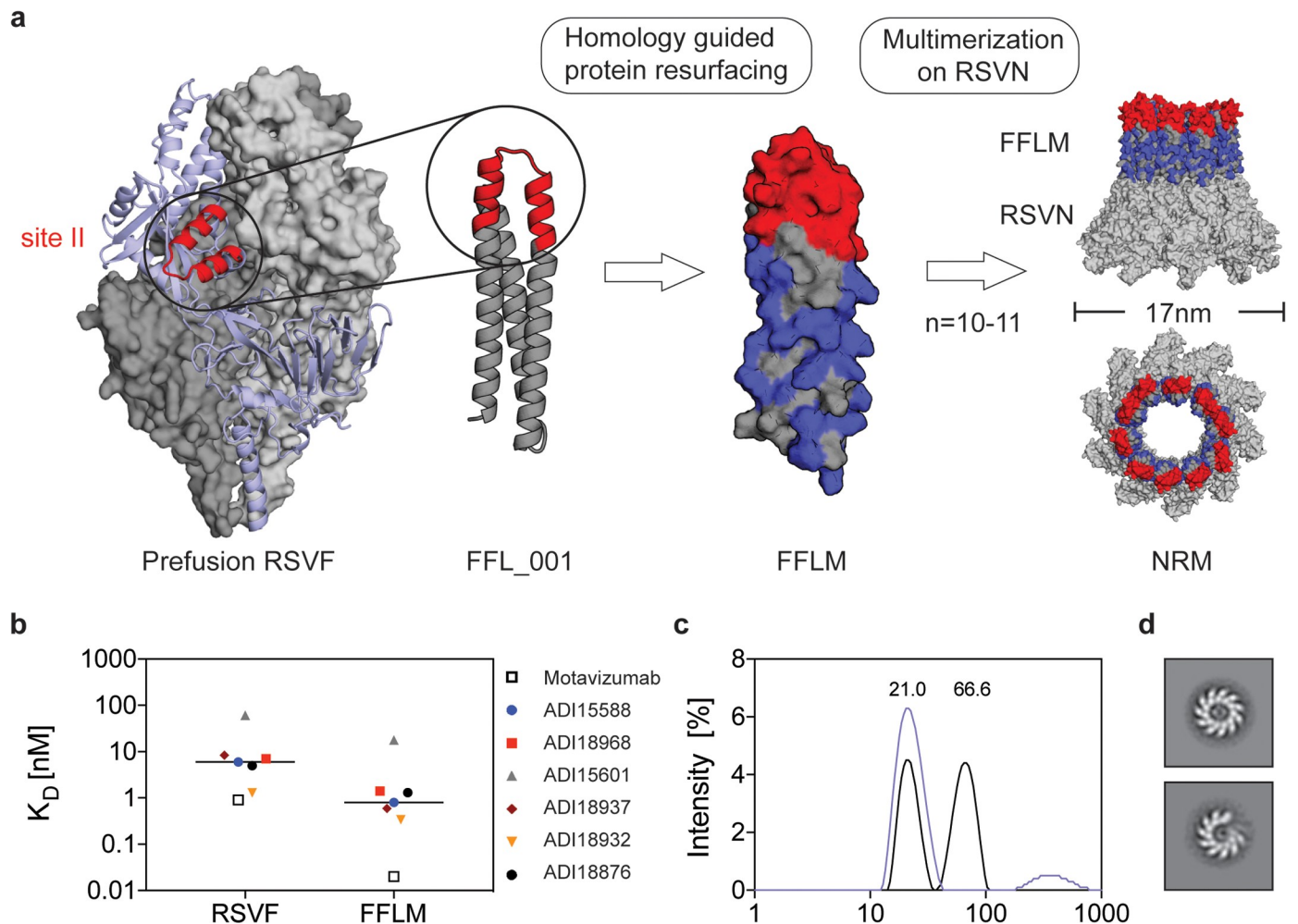


Fig 1. Design of an RSV-based nanoparticle displaying a site II epitope-focused immunogen. (A) Structural model of the prefusion RSVF trimer (PDBID: 4JHW), with two subunits shown as a gray surface and one subunit shown as a light blue cartoon representation with the epitope targeted by palivizumab (antigenic site II) highlighted in red. FFL_001 was previously designed to present the site II epitope in a computationally designed scaffold. FFLM was designed by evolution-guided resurfacing, where changes in amino acid identity are highlighted in blue. FFLM was genetically fused to the N terminus of RSVN, resulting in a high-density array of the epitope-scaffold, as shown by the structural model (based on PDBID: 2WJ8). (B) Kinetic binding affinities of site II-specific human nAbs measured by SPR. K_D s were measured with RSVF/FFLM immobilized as ligand and antibody Fabs as analyte. Sensorgrams and fits are shown in S3 Fig. (C) DLS profiles for FFL_001 and FFLM fused to RSVN. The FFL_001-RSVN fusion protein formed higher-order oligomers in solution (66.6 nm of median diameter), whereas the resurfaced FFLM-RSVN fusion protein (NRM) was monodisperse, with a median diameter of 21 nm. (D) Analysis of the NRM nanoparticles by negative stain electron microscopy. Shown are the 2D class averages of two representative classes. Data are available in S1 Data. DLS, dynamic light scattering; Fab, antibody variable fragment; nAb, neutralizing antibody; PDB, Protein Data Bank; RSV, respiratory syncytial virus; RSVF, RSV fusion protein; RSVN, RSV nucleoprotein; SPR, surface plasmon resonance.

<https://doi.org/10.1371/journal.pbio.3000164.g001>

approximately 21 nm (Fig 1C). Negative stain electron microscopy confirmed the ring-like structure as suggested by the model (Fig 1D). Although we cannot fully rationalize the factors that contributed to the solubility improvement upon multimerization, our strategy to transplant surface residues from a sequence homolog to synthetic proteins may prove useful to enhance the solubility of other computationally designed proteins.

NRM enhances the induction of site II-specific antibodies

We next tested the immunogenicity of NRM and its ability to elicit site II-specific antibodies. Three groups of 10 mice were subjected to three immunizations with 10 μ g of NRM,

monomeric FFLM, and prefusion RSVF [42], which is currently the leading immunogen for an RSV vaccine (Fig 2A). Based on the results of our adjuvant screen (S1 Fig), all the immunogens were formulated in alum. As compared to FFLM, NRM showed a higher overall immunogenicity (directed both against RSVN and FFLM) (Fig 2B).

A key aspect of epitope-focused vaccines is to understand how much of the antibody response targets the viral epitope presented to the immune system. Therefore, we sought to measure the site II-specific antibody titers elicited by NRM and FFLM and compare these epitope-specific antibody responses to those elicited by prefusion RSVF. We established an SPR competition assay (described in the Methods and shown in S4 Fig) to quantify the fraction of site II-specific antibodies elicited by each immunogen (FFLM, NRM, or prefusion RSVF). Briefly, the respective antigen was immobilized on the sensor chip surface, and the fraction of the serum antibody response competed by motavizumab was measured, serving as a proxy for site II-specific antibodies. We observed that NRM elicited site II-specific antibody responses superior to those elicited by RSVF (Fig 2C). This was surprising, given that the ratio of site II epitope surface area to overall immunogen surface is similar in both NRM and RSVF (S2 Fig). To confirm this finding through a direct binding assay rather than a competitive format, we measured the binding levels of sera to the site II epitope in a peptide ELISA, where the site II peptide was immobilized on a streptavidin-coated surface. Peptides mimicking site II are

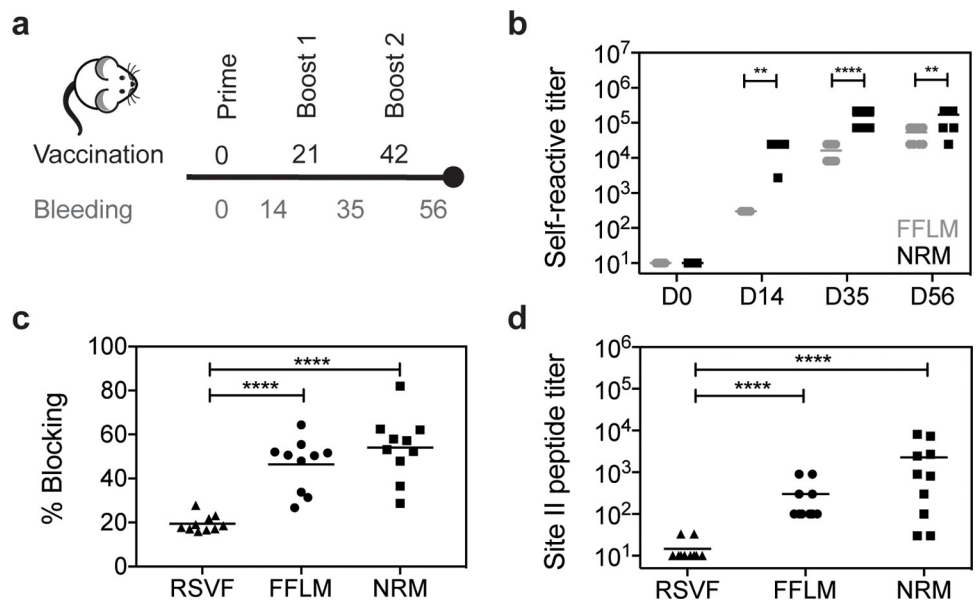


Fig 2. Immunogenicity and quantification of site II-specific antibody responses. (A) Immunization scheme. Balb/c mice were immunized three times on days 0, 21, and 42, and blood was drawn 14 days after each vaccination. (B) Serum antibody titers elicited by FFLM and NRM at different time points measured by ELISA against the respective immunogen. NRM shows significantly increased immunogenicity at days 14, 35, and 56 relative to FFLM. (C) SPR competition assay with motavizumab. Day 56 sera of mice immunized with RSVF, FFLM, or NRM were diluted 1:100, and SPR RU were measured on sensor chip surfaces containing the respective immunogen. Motavizumab binding sites were then blocked by saturating amounts of motavizumab, and the residual serum response was measured to calculate the serum fraction competed by motavizumab binding. Mice immunized with FFLM or NRM show significantly higher levels of serum antibodies that are competed by motavizumab binding. (D) Site II-specific serum titers at day 56 from mice immunized with RSVF, FFLM, and NRM, and NRM, measured by ELISA against site II peptide. Three immunizations with prefusion RSVF elicited low levels of site II-specific antibodies, whereas FFLM and NRM vaccinations yielded significantly higher peptide-specific serum titers. Data shown are derived from at least two independent experiments, with each sample assayed in duplicate. Statistical comparisons were calculated using two-tailed Mann-Whitney U tests. $**p < 0.01$, $***p < 0.0001$, $****p < 0.0001$. Data are available in S1 Data. RSVF, respiratory syncytial virus fusion protein; RU, response units; SPR, surface plasmon resonance.

<https://doi.org/10.1371/journal.pbio.3000164.g002>

known to be conformationally flexible [43] (S5 Fig) but have been shown to adopt a very similar conformation upon antibody binding to the one presented in the context of pre- and postfusion RSVF [44]. Consistent with the previous experiment, we found that NRM elicited site II-specific responses that were two orders of magnitude higher than those of RSVF (Fig 2D). Together, we concluded that an epitope-focused immunogen, despite similar molecular surface area, can elicit substantially higher levels of site-specific antibodies compared to a viral fusion protein.

NRM induces low levels of RSVF cross-reactive antibodies with low neutralization potency

Given the substantial site II peptide-specific serum titers elicited by NRM in mice, we investigated whether these antibodies cross-reacted with prefusion RSVF and were sufficient to neutralize RSV *in vitro*.

Following three immunizations with NRM, all the mice ($n = 10$) developed detectable serum cross-reactivity with prefusion RSVF (mean serum titer = 980) (Fig 3A). Sera also cross-reacted with the postfusion conformation of RSVF (mean serum titer = 380), but binding to virus-infected cell lysate was negligible for mice immunized with the epitope-scaffold (S6 Fig). The overall quantity of RSVF cross-reactive antibodies elicited by immunization with an immunogen presenting a single epitope was found to be more than two orders of magnitude lower than those of mice immunized with prefusion RSVF, which comprises at least six antigenic sites [5]. Similarly, a B cell enzyme-linked immunospot assay (ELISpot) revealed that NRM-immunized mice presented prefusion RSVF-reactive antibody-secreting cells, but their frequency was approximately one order of magnitude lower than it was upon immunization with prefusion RSVF (Fig 3C).

The major determinant for antibody specificity is attributed to the heavy chain complementarity-determining region 3 (HCDR3) [45]. Whereas for certain classes of nAbs the antibody lineages and their sequence features are well-defined (e.g., HIV neutralizing VRC01 class antibodies [46] or RSV-neutralizing MPE8-like antibodies [47]), antibodies targeting RSV antigenic site II seem to be derived from diverse precursors and do not show HCDR3 sequence convergence in humans [5]. Although we did not expect to find dominant lineages or HCDR3 sequence patterns in mice, we used next-generation antibody repertoire sequencing (NGS) [48] to ask whether NRM could elicit antibodies with similar sequence signatures to those elicited by prefusion RSVF. Indeed, we found 300 clonotypes, defined as antibodies derived from the same VH gene with the same HCDR3 length and 80% sequence similarity, that overlapped between NRM and the prefusion RSVF-immunized cohort, suggesting that at the molecular level, relevant antibody lineages can be activated with the NRM immunogen (S7 Fig). Nine out of the 20 most expanded clonotypes in the NRM cohort were also present in mice immunized with prefusion RSVF, albeit not as expanded (Fig 3B). This finding might reflect the enrichment of site II-specific antibodies in the NRM cohort (Fig 2D).

We further investigated whether these low levels of prefusion RSVF-binding antibodies were sufficient to neutralize RSV *in vitro*. Although three immunizations with prefusion RSVF elicited potent RSV-neutralizing serum titers (mean $IC_{50} = 10,827$), for NRM we only detected low levels of RSV-neutralizing serum activity in three out of 10 mice (Fig 3D). This result is consistent with that of Correia and colleagues [22], who observed no serum neutralization in mice but succeeded in inducing nAbs in NHPs with prior RSV seronegativity.

Altogether, we concluded that despite NRM's superior potential to induce high levels of site II-specific antibodies, the majority of antibodies activated from the naïve repertoire are not functional for RSV neutralization. A potential explanation, stemming from structural

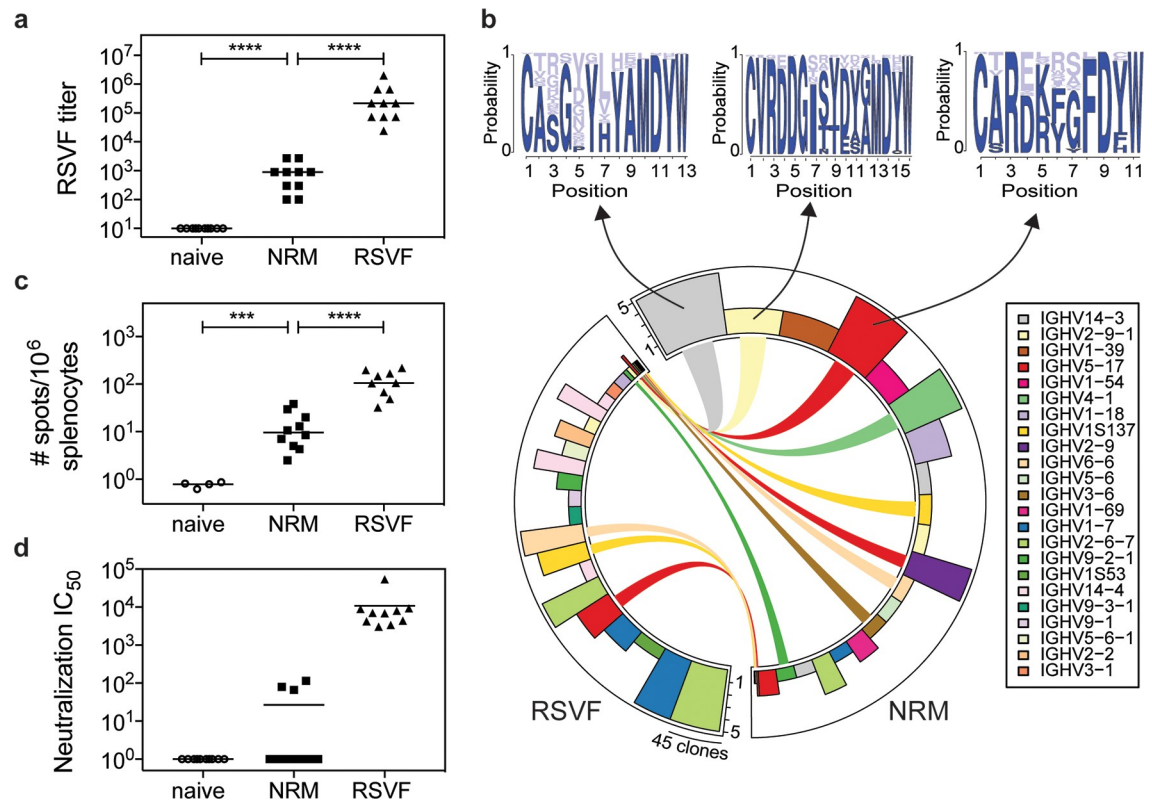


Fig 3. RSVF cross-reactivity and serum neutralization. (A) NRM elicits prefusion RSVF cross-reactive serum levels, the quantity of which is two orders of magnitude lower compared to that elicited by prefusion RSVF immunization. Mice immunized only with adjuvant (naïve) do not show RSVF cross-reactivity. (B) Next-generation sequencing of antibody repertoire. Antibody variable heavy chains of mice immunized with RSVF or NRM (5 mice per cohort) were sequenced at day 56 and grouped into clonotypes. The circos plot shows the 20 most expanded clonotypes from both cohorts, with identical clonotypes connected. Height of bars indicates number of mice that showed the respective clonotype; width represents the clonal expansion within a clonotype (i.e., the number of clones grouped into the respective clonotype). Three clonotypes that occurred both in the RSVF and the NRM cohort but were expanded within the NRM cohort were analyzed for their HCDR3 sequence profile, as shown by sequence logo plots (top). Dark blue color represents amino acid identities that occurred in RSVF cohort; light blue color represents amino acids uniquely found following NRM immunization. The frequency of each amino acid in the NRM cohort is indicated by the size of the letter. (C) B cell ELISpot of mouse splenocytes to quantify prefusion RSVF-specific ASCs. Number of ASCs per 10^6 splenocytes that secrete prefusion RSVF-specific antibodies following three immunizations with adjuvant only (naïve), NRM, or prefusion RSVF. (D) RSV-neutralizing activity of mouse sera from day 56 shown as neutralization IC_{50} . Three out of 10 mice immunized with NRM showed detectable RSV-neutralizing activity, whereas all mice immunized with prefusion RSVF neutralized RSV (mean $IC_{50} = 10,827$). Data shown are from one out of two independent experiments. Statistical comparisons were calculated using two-tailed Mann-Whitney U tests. $***p < 0.001$, $****p < 0.0001$. Data are available in [S1 Data](#). ASC, antibody-secreting cell; ELISpot, enzyme-linked immunospot assay; HCDR3, heavy chain complementarity-determining region 3; IGHV, immunoglobulin heavy chain variable gene; RSV, respiratory syncytial virus; RSVF, RSV fusion protein.

<https://doi.org/10.1371/journal.pbio.3000164.g003>

comparison between the epitope-focused immunogen and RSVF, is that these antibodies do not recognize the site II epitope in its native, quaternary environment in prefusion RSVF or in virions in sufficient amounts and with high enough affinity to potentially neutralize RSV.

NRM boosts site II-specific antibodies under conditions of preexisting immunity

Although vaccination studies in naïve animal models are an important first step to validate novel immunogens, previous studies [22] and results presented here imply that epitope-scaffolds may not be able to elicit robust RSV-neutralizing serum activity from a naïve antibody repertoire. However, given the high affinity of the epitope-scaffold toward a panel of site II-

specific nAbs, together with the ability to elicit high titers of site II-specific antibodies in vivo, we hypothesized that such an epitope-focused immunogen could be efficient in recalling site II-specific B cells in a scenario of preexisting immunity, thereby achieving an enhanced site-specific neutralization response.

Our initial immunization studies with prefusion RSVF showed that site II-specific responses were subdominant (Fig 2C and 2D). Given that subdominance is a common immunological phenotype for many of the neutralization epitopes that are relevant for vaccine development [49], we sought to test if NRM could boost subdominant antibody lineages that should ultimately be functional and recognize the epitope in the quaternary environment of the viral protein. To test this hypothesis, we designed a mouse immunization experiment with three cohorts, as outlined in Fig 4A. Following a priming immunization with RSVF, cohort 1 was boosted with adjuvant only (“prime-only”), cohort 2 received two boosting immunizations with prefusion RSVF (“homologous boost”), and cohort 3 received two boosts with NRM (“heterologous boost”).

A comparison between the prefusion RSV-immunized groups prime-only and homologous boost revealed that the two additional boosting immunizations with RSVF only slightly increased overall titers of prefusion RSVF-specific antibodies ($p = 0.02$), indicating that a single immunization with adjuvanted RSVF is sufficient to induce close to maximal serum titers against RSVF (Fig 4B). Following the heterologous boost with NRM, overall RSVF-specific antibody titers remained statistically comparable to the prime-only group ($p = 0.22$).

Next, we quantified the site II-specific endpoint serum titers in a peptide ELISA format (Fig 4C). The homologous boost with prefusion RSVF failed to increase site II-specific antibody levels, reducing the responses directed to site II to the lower limit of detection by ELISA. This result is yet another example of the underlying complexity inherent to the fine specificity of antibody responses elicited by immunogens and how important specificities can be dampened throughout the development of an antibody response. In contrast to the homologous boost, the heterologous boost with NRM significantly increased site II peptide-specific serum titers ($p < 0.0001$).

In order to understand whether this increase relied at least partially on an actual recall of antibodies primed by RSVF, or rather on an independent antibody response irrelevant for RSVF binding and RSV neutralization, we dissected the epitope specificity within the RSVF-specific serum response. In an SPR competition assay, a significantly higher fraction ($p = 0.02$) of prefusion RSVF-reactive antibodies were competed by motavizumab in mouse sera primed with prefusion RSVF and boosted with NRM (mean percent blocking = $37.5\% \pm 14.5\%$), as compared to mice immunized once or three times with prefusion RSVF ($21.5\% \pm 12.1\%$ or $19.5\% \pm 3.7\%$, respectively) (Fig 4D). Control mice immunized that were not primed with prefusion RSVF and instead were immunized three times with NRM did not yield detectable binding signals against prefusion RSVF in an SPR assay, despite detectable ELISA signals (Fig 3A). Thus, while the heterologous boost with NRM will also prime antibodies that do not bind RSVF, the increased fraction of prefusion RSVF-binding, site II-specific antibodies is likely to arise from a recall of RSVF-primed, site II-specific antibodies. Similarly, a competition ELISA revealed that a significantly larger fraction of overall RSVF reactivity was attributed to site II-specific antibodies upon heterologous boost, as compared to both control groups (mean percent competition = $36.1\% \pm 2.5\%$ versus $22.6\% \pm 9.1\%$ or $14.4\% \pm 5.9\%$, respectively, $p = 0.002$ and $p < 0.0001$). In contrast, site II-specific antibodies were significantly higher in mice that received only one as opposed to three RSVF immunizations, indicating that RSVF boosting immunizations further dampened site II-specific antibody titers ($p = 0.03$) (Fig 4E).

Together, we have shown that the serum antibody specificity can be steered toward a well-defined antigenic site by boosting preexisting, subdominant antibody levels with an epitope-

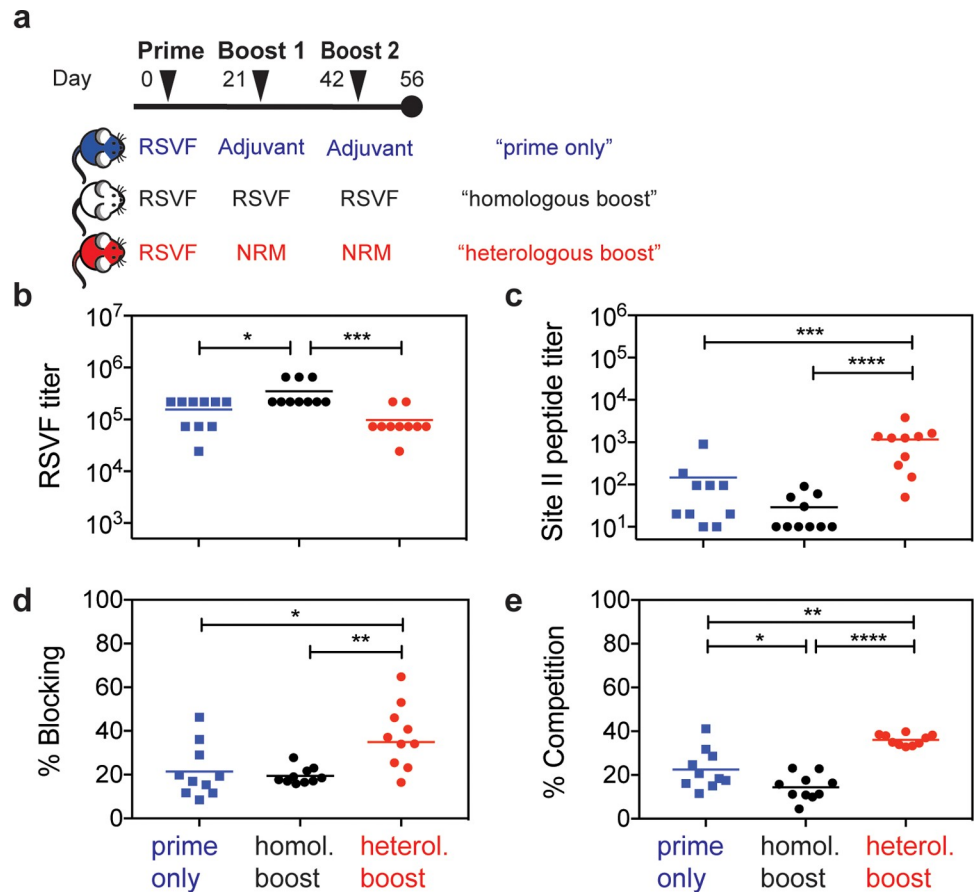


Fig 4. Heterologous prime-boost reshapes antibody responses enhancing levels of site II-specific antibodies. (A) Heterologous prime-boost study groups. Three mouse cohorts were immunized with either 1x RSVF (“prime-only”), 3x RSVF (“homologous boost”), or 1x RSVF followed by two boosts with NRM (“heterologous boost”). (B) Antibody titers directed against prefusion RSVF. Mice receiving homologous boosting immunizations show slightly higher RSVF-specific serum titers compared to the prime-only cohort, whereas heterologous boosting yielded statistically comparable titers to the prime-only group. The difference between the homologous and heterologous boost cohorts was statistically significant. (C) Site II-specific titers measured by ELISA showed that the heterologous boost significantly increases site II-specific titers compared to both prime and homologous boost groups. Albeit not statistically significant ($p = 0.06$), mice receiving a homologous boost had lower levels of site II-specific antibodies compared to prime-only group. (D) SPR competition assay with motavizumab on a prefusion RSVF-coated sensor chip. Sera from indicated groups were diluted 1:100, and RSVF binding responses were quantified. Site II was then blocked with motavizumab, and the remaining serum response was quantified. The heterologous (“heterol.”) boost induced a significantly higher fraction of site II-directed antibodies that competed with motavizumab for RSVF binding, as compared to both prime-only and homologous (“homol.”) boost groups. (E) Quantification of site II-specific responses in a competition ELISA. Binding was measured against prefusion RSVF, and the AUC was calculated in the presence of RSVN competitor, normalized to the AUC in the presence of RSVN as a control competitor. Compared to the prime-only group, the homologous boost resulted in significantly lower site II-specific serum titers, confirming the trend observed in (C). The heterologous boost increased the fraction of site II-targeting antibodies within the pool of prefusion RSVF-specific antibodies compared to both control groups. Data presented are from at least two independent experiments, with each sample assayed in duplicates. Statistical comparisons were calculated using two-tailed Mann-Whitney U tests. * $p < 0.05$, ** $p < 0.01$, *** $p < 0.0001$, **** $p < 0.0001$. Data are available in [S1 Data](#). AUC, area under the curve; RSVF, RSV fusion protein; RSVN, RSV nucleoprotein; SPR, surface plasmon resonance.

<https://doi.org/10.1371/journal.pbio.3000164.g004>

focused immunogen. This is an important and distinctive feature of the epitope-focused immunogen compared to an immunogen based on a viral protein (prefusion RSVF), which was shown to decrease already subdominant antibody responses under the same conditions.

These results may have broad implications for strategies to control antibody fine specificities in vaccination schemes, both for RSV and other pathogens.

Boosted antibodies neutralize RSV in vitro

The enhanced reactivity to site II observed in the heterologous prime–boost scheme led us to investigate if the antibodies boosted by a synthetic immunogen were functionally relevant for virus neutralization. In bulk sera, we observed 2.3-fold higher serum neutralization titers in mice receiving the heterologous boost (mean IC₅₀ = 7,654) compared to the prime-only control group (mean IC₅₀ = 3,275) (Fig 5A). Although this increase in serum neutralization was not statistically significant, we next assessed if this increase in neutralization was driven by increased levels of epitope-specific antibodies. We observed that site II–directed antibody levels correlated with overall serum neutralization titers in the heterologous prime–boost group

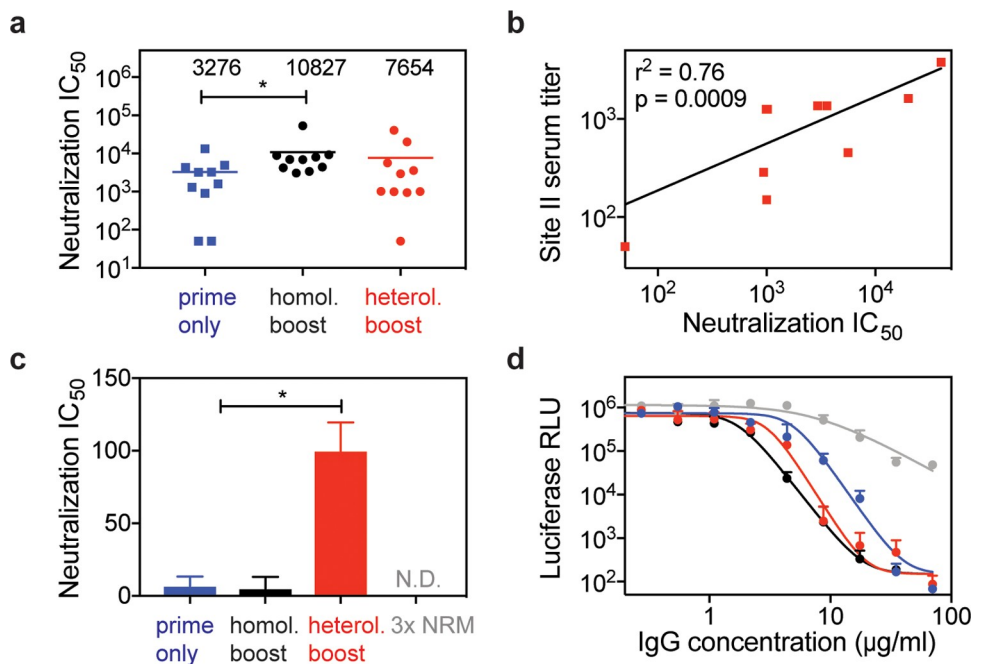


Fig 5. Boosted site II–specific antibodies are functional and mediate increased neutralization activity. (A) In vitro RSV neutralization IC₅₀ for each group. Compared to the prime-only group, mice receiving a homologous (“homol.”) boost showed increased RSV neutralization titers. On average, the heterologous (“heterol.”) boost yielded a 2.3-fold increase in serum neutralization titers compared to prime-only, but these differences were statistically not significant when compared to either group. (B) Correlation of site II–specific serum titer (measured by peptide ELISA) with RSV neutralization IC₅₀ as determined for each mouse within the heterologous prime–boost cohort. Correlations for control groups are shown in S8 Fig. Data represent the mean of two independent experiments, each measured in duplicate. Pearson correlation coefficient (r^2) and p -value were calculated in GraphPad Prism. (C) Serum fractionation revealed increased levels of site II–mediated neutralization. Site II–specific antibodies from mouse sera were enriched in an affinity purification as described in the Methods and shown in S9 Fig. The IC₅₀ values are the dilution factor of site II–specific antibodies eluted and quantify the total site II–mediated neutralization. Antibodies purified from the heterologous boost group showed a 15-fold increase in RSV–neutralizing activity compared to the prime-only and homologous boost control groups. No site II–mediated neutralization was detected for mice receiving three immunizations of NRM. (D) RSV neutralization potency of affinity-purified site II–specific antibodies. Purified antibodies from each group were diluted to a concentration of 70 µg/ml to measure their RSV neutralization potencies. Site II antibodies from prime-only, heterologous boost, and homologous boost exhibited similar neutralization potencies (IC₅₀ = 4.9 µg/ml, IC₅₀ = 3.0 µg/ml, and IC₅₀ = 1.7 µg/ml, respectively). Data are presented from two independent experiments, and each sample was assayed in duplicate with additional controls shown in S9 Fig. Statistical comparisons were calculated using two-tailed Mann-Whitney U tests. * $p < 0.05$. Data are available in S1 Data. IgG, immunoglobulin G; N.D., nondetectable; RLU, relative light units; RSV, respiratory syncytial virus.

<https://doi.org/10.1371/journal.pbio.3000164.g005>

($r^2 = 0.76$, $p = 0.0009$) (Fig 5B), whereas the prime-only ($r^2 = 0.32$, $p = 0.09$) or the homologous boost cohorts showed no such correlation ($r^2 = 0.18$, $p = 0.22$) (S8 Fig).

To characterize the RSV-neutralizing activity mediated by site II-specific antibodies, we pooled sera from each cohort, enriched site II-specific antibodies, and measured viral neutralization (see Methods and S9 Fig). Briefly, we incubated pooled sera from each group with streptavidin beads, which were conjugated to biotin-labeled antigenic site II peptide, and eluted bound antibodies. To control for the quality of the enrichment protocol, we verified by ELISA that the column flow-through was depleted of site II-specific antibodies (S9 Fig). In agreement with the different site II peptide-specific serum levels shown in Fig 4, the overall quantity of site II-specific antibodies purified from equivalent amounts of sera differed between groups, with the heterologous boost and the 3x NRM groups showing the highest levels (S9 Fig).

Next, we tested neutralization of this polyclonal pool of site II-specific antibodies. We found that the heterologous boost cohort showed a 15-fold greater site II-specific neutralization titer ($IC_{50} = 99.6$) as compared to the prime-only and homologous boost cohorts ($IC_{50} = 6.6$ and $IC_{50} = 4.9$, respectively). It is important to note that although the homologous boost with RSVF showed increased serum neutralizing activity compared to the prime-only control group, site II-mediated neutralization was similar. This finding is consistent with our observation that site II-specific antibodies do not increase with repeated immunizations of prefusion RSVF. Enriched antibodies from the 3x NRM group were nonneutralizing, despite the high concentration of site II-specific antibodies (S9 Fig). Thus, NRM significantly enhances site II-mediated RSV neutralization but requires the priming of a relevant subset of RSVF-binding antibodies. Finally, we addressed whether this increase in site II-mediated neutralization was due to higher amounts of site II-specific antibodies or the intrinsic neutralization potency of the same antibodies. As shown in Fig 5D, antibodies from the prime-only, heterologous boost, and homologous boost cohorts exhibit similar neutralization potencies (IC_{50} ranging from 1.7 $\mu\text{g/ml}$ to 4.9 $\mu\text{g/ml}$) of site II-specific antibodies. Consequently, the heterologous boosting scheme yielded higher amounts of site-specific, functional antibodies, rather than an increased potency of the same antibodies.

Altogether, we dissected the mode of action of the synthetic immunogens when used as heterologous boosters, in which the observed enhanced neutralization resulted from the increase of sheer amounts of antibodies directed to site II.

Discussion

Despite a rapid increase in our atomic-level understanding of antibody-antigen interactions for various pathogens, the translation of structural information into efficacious immunogens that elicit antibody responses specific to bona fide epitopes remains a key challenge for next-generation vaccine development.

Multiple strategies have been investigated to focus nAb responses on defined neutralization epitopes [50]. Among them, epitope-scaffolds have been shown to elicit RSV site II-specific nAb responses in naïve NHPs. Although the overall serum neutralization was modest, a monoclonal antibody induced by vaccination showed superior neutralization potency to that of palivizumab [22]. However, a major limitation of epitope-scaffold immunogens [43, 51, 52] is that the quaternary environment of the epitope presented in the native viral protein is lost. Thus, the binding mode of a significant fraction of the elicited antibodies is likely incompatible with the epitope in its native environment. This observation is reinforced by our finding that although NRM elicited high serum levels of site II peptide-specific antibodies, only low levels were cross-reactive with RSVF, and neutralizing activity was residual. This finding is consistent with previous studies using epitope-scaffolds [43, 53, 54]. Together, these results highlight

the limitations of synthetic scaffolds in an epitope-focused vaccine approach in naïve individuals.

However, our finding—that an epitope that is subdominant (site II) in its native environment (prefusion RSVF) is readily targeted by the immune system when presented in a distinct molecular context (NRM)—supported the potential use of synthetic immunogens to reshape antibody responses toward such well-defined antigenic sites. Preexisting immunity against a viral protein (RSVF, influenza HA, or others), in which certain antibody specificities are subdominant, is a common scenario in humans that have encountered repeated natural infections throughout their life [27, 55–57]. Therefore, a major challenge for vaccine development is to boost preexisting, subdominant antibodies and enhance site-specific neutralization.

To date, boosting nAbs that target specific epitopes under conditions of preexisting immunity has been challenging. For instance, strong antibody responses against immunodominant epitopes can sterically mask the neutralization epitope, preventing the induction of a potent antibody response targeting the subdominant site [24, 26, 27, 58]. Overcoming these established immunodominance hierarchies is complex, as such hierarchies seem to be impacted by multiple factors, including serological antibody levels, their specificity, memory B cell counts, adjuvants, and the immunization or infection route [25].

Heterologous prime–boost schemes are a promising strategy to guide the fine specificity of antibody responses and to focus these responses on vulnerable antigenic sites. Several vaccine studies have been conducted for influenza [34, 35], RSV [32], and HIV [29], in which the heterologous immunogens were alternative strains or modified viral fusion proteins but yet not as heterologous as a computationally designed epitope-scaffold. It is possible that immunogens based on modified viral proteins retain immunodominant signatures that steer antibody responses away from the target epitopes. Although this scenario may not be fully absent in synthetic epitope-scaffolds, it is at least mitigated by the fact that the protein has not evolved under the pressure of escaping the immune system.

Our study demonstrates that a heterologous boosting immunogen that optimally presents a single neutralization epitope can boost preexisting, subdominant antibody responses that target this epitope, yielding increased epitope-mediated neutralization. The ability to narrowly focus antibody responses to a single epitope that mediates clinical protection underlines the potential of rationally designed immunogens for vaccine development against elusive pathogens. In particular, our results demonstrate that although single-epitope immunogens may not be the most powerful to select functional antibodies from a naïve repertoire, they have a unique ability to boost neutralizing epitope-specific antibodies primed by a viral protein. Further studies in more relevant animal models will reveal if nAbs primed by natural infection with RSV can also be boosted, mimicking a more realistic vaccination scenario.

Given that the approach presented here is generalizable and that epitope-scaffold nanoparticles can be proven successful in boosting nAbs specific for other sites, this strategy holds great potential to tune levels of antibody specificities through heterologous prime–boost vaccination schemes, which are now frequently used for challenging pathogens [29, 34, 59].

The original antigenic sin theory in the influenza field describes that the first viral exposure permanently shapes the antibody response, which causes individuals to respond to seasonal vaccines in a manner dependent on their immune history [24, 60]. Seasonal vaccines generally fail to boost antibodies targeting broadly neutralization epitopes on the HA stem region [24]. Focusing antibody responses on these defined epitopes may remove the need for annual vaccine reformulation and may also protect against emerging pandemic strains [14, 49, 61, 62]. The influenza vaccine challenge seems particularly well suited to our approach, considering that the human population has preexisting immunity to influenza, including some subdominant bnAbs that seasonal vaccines fail to stimulate [24].

Lastly, vaccine development against antigenically related viruses such as Zika and dengue could benefit from the approach presented here, as antibodies mounted against the envelope protein of a dengue subtype can facilitate infection with Zika [63] or other dengue subtypes [64]. A site conserved between all four dengue subtypes and Zika envelope protein has been structurally characterized and suggested for the development of an epitope-focused immunogen [7].

When seeking to apply an immunofocusing strategy to other antigenic sites and pathogens, one challenge is the development of epitope-scaffolds stably presenting the epitope in a synthetic immunogen that is compatible with antibody binding. Whereas the RSV antigenic site II is a structurally simple helix-turn-helix motif, many other identified neutralization epitopes comprise multiple, discontinuous segments. However, continuous advances in rational protein design techniques [65] will allow the design of more complex protein scaffolds to stabilize increasingly complex epitopes.

Altogether, we have shown how an optimized presentation of a computationally designed immunogen in an RSVN-based nanoparticle can reshape bulk serum responses and boost subdominant nAb responses in vivo. This is a distinctive feature compared to using prefusion RSVF as a boosting immunogen and underscores how subdominant epitopes can be converted to immunodominant epitopes when presented in a different environment. We foresee the great promise of this strategy to overcome the challenge of boosting and focusing preexisting immunity toward defined neutralization epitopes, potentially applicable to multiple pathogens.

Methods

Ethics statement

All animal experiments were approved by the Veterinary Authority of the Canton of Vaud (Switzerland) according to Swiss regulations of animal welfare (animal protocol number 3074).

Resurfacing

The previously published RSV site II epitope-scaffold (“FFL_001”) [22] was designed based on a crystal structure of a mutant of ribosome recycling factor from *E. coli* (PDB entry IISE). Using BLAST, we identified sequence homologs of IISE from eukaryotic organisms and created a multiple-sequence alignment with clustal omega (CLUSTALO [1.2.1]) [66] of the mouse homolog sequence (NCBI reference NP_080698.1), IISE, and FFL_001. Surface-exposed residues of FFL_001 were then mutated to the respective residue of the mouse homolog using the Rosetta fixed backbone design application [40], resulting in 38 surface mutations. Amino acid changes were verified to not impact overall Rosetta energy score term.

Protein expression and purification

FFLM. DNA sequences of the epitope-scaffold designs were purchased from Genscript and cloned in pET29b, in frame with a C-terminal 6x His tag. The plasmid was transformed in *E. coli* BL21 (DE3) and grown in Terrific Broth supplemented with kanamycin (50 µg/ml). Cultures were inoculated to an OD₆₀₀ of 0.1 from an overnight culture and incubated at 37°C. After reaching an OD₆₀₀ of 0.6, expression was induced by the addition of 1 mM isopropyl-β-D-thiogalactoside (IPTG), and cells were incubated for a further 4–5 hours at 37°C. Cell pellets were resuspended in lysis buffer (50 mM TRIS [pH 7.5], 500 mM NaCl, 5% Glycerol, 1 mg/ml lysozyme, 1 mM PMSF, 1 µg/ml DNase) and sonicated on ice for a total of 12 minutes, in intervals of 15-second sonication followed by a 45-second pause. Lysates were clarified by centrifugation (18,000 rpm, 20 minutes), sterile-filtered, and purified using a His-Trap FF column on an Äkta pure system (GE Healthcare). Bound proteins

were eluted in buffer containing 50 mM Tris, 500 mM NaCl, and 300 mM imidazole (pH 7.5). Concentrated proteins were further purified by size-exclusion chromatography on a Superdex 75 300/10 (GE Healthcare) in phosphate-buffered saline (PBS). Protein concentrations were determined by measuring the absorbance at 280 nm on a Nanodrop (Thermo Scientific). Proteins were concentrated by centrifugation (Millipore, #UFC900324) to 1 mg/ml, snap frozen in liquid nitrogen, and stored at -80°C .

NRM. The full-length N gene (sequence derived from the human RSV strain Long, ATCC VR-26; GenBank accession number AY911262.1) was PCR amplified using the Phusion DNA polymerase (Thermo Scientific) and cloned into pET28a+ at NcoI-XhoI sites to obtain the pET-N plasmid. The sequence of FFLM was then PCR amplified and cloned into pET-N at NcoI site to the pET-NRM plasmid. *E. coli* BL21 (DE3) bacteria were cotransformed with pGEX-PCT [67] and pET-FFLM-N plasmids and grown in LB medium containing ampicillin (100 $\mu\text{g}/\text{ml}$) and kanamycin (50 $\mu\text{g}/\text{ml}$). The same volume of LB medium was then added, and protein expression was induced by the addition of 0.33 mM IPTG to the medium. Bacteria were incubated for 15 hours at 28°C and then harvested by centrifugation. For protein purification, bacterial pellets were resuspended in lysis buffer (50 mM Tris-HCl [pH 7.8], 60 mM NaCl, 1 mM EDTA, 2 mM dithiothreitol, 0.2% Triton X-100, 1 mg/ml lysozyme) supplemented with a complete protease inhibitor cocktail (Roche), incubated for 1 hour on ice, and disrupted by sonication. The soluble fraction was collected by centrifugation at 4°C for 30 minutes at 10,000g. Glutathione-Sepharose 4B beads (GE Healthcare) were added to clarify supernatants and incubated at 4°C for 15 hours. The beads were then washed one time in lysis buffer and two times in 20 mM Tris (pH 8.5), 150 mM NaCl. To isolate NRM, beads containing bound complex were incubated with thrombin for 16 hours at 20°C . After cleavage of the GST tag, the supernatant was loaded onto a Sephacryl S-200 HR 16/30 column (GE Healthcare) and eluted in 20 mM Tris-HCl, 150 mM NaCl (pH 8.5).

Antibody variable fragments (Fabs). For Fab expression, heavy and light chain DNA sequences were purchased from Twist Biosciences and cloned separately into the pHLSec mammalian expression vector (Addgene, #99845) using AgeI and XhoI restriction sites. Expression plasmids were premixed in a 1:1 stoichiometric ratio, cotransfected into HEK293-F cells, and cultured in FreeStyle medium (Gibco, #12338018). Supernatants were harvested after 1 week by centrifugation and purified using a kappa-select column (GE Healthcare). Elution of bound proteins was conducted using 0.1 M glycine buffer (pH 2.7), and eluates were immediately neutralized by the addition of 1 M Tris ethylamine (pH 9), followed by buffer exchange to PBS (pH 7.4).

Prefusion RSVF. Protein sequence of prefusion RSVF corresponds to the sc9-10 DS-Cav1 A149C Y458C S46G E92D S215P K465Q variant designed by Joyce and colleagues [42], which we refer to as RSVF DS2. RSVF DS2 was codon optimized for mammalian expression and cloned into the pHCMV-1 vector together with two C-terminal Strep-Tag II and one 8x His tag. Plasmids were transfected in HEK293-F cells and cultured in FreeStyle medium. Supernatants were harvested 1 week after transfection and purified via Ni-NTA affinity chromatography. Bound protein was eluted using buffer containing 10 mM Tris, 500 mM NaCl, and 300 mM Imidazole (pH 7.5), and eluate was further purified on a StrepTrap HP affinity column (GE Healthcare). Bound protein was eluted in 10 mM Tris, 150 mM NaCl and 20 mM desthiobiotin (pH 8) (Sigma) and size excluded in PBS (pH 7.4) on a Superdex 200 Increase 10/300 GL column (GE Healthcare) to obtain trimeric RSVF.

Negative-stained sample preparation, data acquisition, and image processing

NRM was size excluded in PBS on a Superose 6 column (GE Healthcare) and diluted to a concentration of 0.015 mg/ml. The sample was adsorbed to a glow-discharged carbon-coated copper grid (EMS, Hatfield, PA, United States) washed with deionized water and stained with a solution of uranyl formate 0.75%. Observation was made using an F20 electron microscope (Thermo Fisher, Hillsboro, OR, USA) operated at 200 kV. Digital images were collected using a direct detector camera Falcon III (Thermo Fisher, Hillsboro, OR, USA) 4,098 × 4,098 pixels. Automatic data collection was performed using EPU software (Thermo Fisher, Hillsboro, OR, USA) at a nominal magnification of 50,000×, corresponding to a pixel size of 2 Å, and defocus range of −1 μm to −2 μm.

Contrast transfer function for each image was estimated using CTFFIND4 [68]. One thousand particles of nanorings were picked using XMIPP manual-picking utility within SCIPION framework [69]. Manually picked particles were used as input into XMIPP auto-picking utility, resulting in 13,861 particles. Particles were extracted and binned to have the box size of 100 pixels, corresponding to the pixel size of 4 Å; phase-flipped; and subjected for three rounds of reference-free 2D classification without contrast transfer function correction in RELION-3.0 Beta [70].

Affinity determination using SPR

SPR experiments were performed on a Biacore 8K at room temperature with HBS-EP+ running buffer (10 mM HEPES [pH 7.4], 150 mM NaCl, 3 mM EDTA, 0.005% v/v Surfactant P20) (GE Healthcare). Approximately 100 response units (RU) of FFLM were immobilized via amine coupling on a CM5 sensor chip (GE Healthcare). Serial dilutions of site II-specific Fabs were injected as analyte at a flow rate of 30 μl/minute with 120 seconds of contact time. Following each injection cycle, ligand regeneration was performed using 0.1 M glycine (pH 2). If not stated otherwise, data analysis was performed using 1:1 Langmuir binding kinetic fits within the Biacore evaluation software (GE Healthcare).

Mouse immunizations

Six-week-old, female Balb/c mice were ordered from Janvier labs and acclimatized for 1 week. Immunogens were thawed on ice and diluted in PBS (pH 7.4) to a concentration of 0.2 mg/ml. The immunogens were then mixed with an equal volume of 2% Alhydrogel (Invivogen), resulting in a final Alhydrogel concentration of 1%. Other adjuvants were formulated according to manufacturer's instructions. After mixing immunogens and adjuvants for 1 hour at 4°C, each mouse was injected with 100 μl, corresponding to 10 μg immunogen adsorbed to Alhydrogel. All immunizations were done subcutaneously, with no visible irritation around the injection site. Immunizations were performed on days 0, 21, and 42. Blood (100–200 μl) was drawn on days 0, 14, and 35, and the maximum amount of blood (200–1,000 μl) was taken by cardiac puncture at day 56, when mice were euthanized.

Antigen ELISA

Nunc MediSorp plates (Thermo Scientific, #467320) were coated overnight at 4°C with 100 μl of antigen (recombinant RSVF, FFLM, and NRM) diluted in coating buffer (100 mM sodium bicarbonate [pH 9]) at a final concentration of 0.5 μg/ml. For blocking, plates were incubated for 2 hours at room temperature with blocking buffer (PBS + 0.05% Tween 20 [PBST]) supplemented with 5% skim milk powder [Sigma, #70166]). Mouse sera were serially diluted in

blocking buffer and incubated for 1 hour at room temperature. Plates were washed five times with PBST before adding 100 μ l of anti-mouse HRP-conjugated secondary antibody diluted at 1:1,500 in blocking buffer (Abcam, #ab99617). An additional five washes were performed before adding Pierce TMB substrate (Thermo Scientific, #34021). The reaction was stopped by adding 100 μ l of 2 M sulfuric acid, and absorbance at 450 nm was measured on a Tecan Safire 2 plate reader. Each plate contained a standard curve of motavizumab to normalize signals between different plates and experiments. Normalization was done in GraphPad Prism. The mean value was plotted for each cohort, and statistical analysis was performed using GraphPad Prism.

Whole-virus ELISA

Nunc MaxiSorp ELISA plates (Thermo Scientific, #44-2404-21) were coated with heat-inactivated, frozen-thawed cell lysates from Hep2 cells that were infected for 48 hours with RSV [37]. A control lysate was prepared from uninfected Hep2 cells to subtract background signals. ELISA was performed as described for the antigen ELISA.

Competition ELISA

Prior to incubation with a coated antigen plate, sera were serially diluted in the presence of 100 μ g/ml competitor antigen and incubated overnight at 4°C. ELISA curves of a positive control, motavizumab, are shown in S10 Fig. Curves were plotted using GraphPad Prism, and the area under the curve (AUC) was calculated for the specific (NRM) and control (RSVN) competitor. Percent competition was calculated using the following formula [71]:

$$\% \text{ competition} = \left(1 - \left(\frac{\text{AUC}(\text{specific competitor (NRM)})}{\text{AUC}(\text{control competitor (NR)})} \right) \right) * 100$$

Peptide sandwich ELISA

The antigenic site II was synthesized as peptide by JPT Peptide Technologies, Germany. The following sequence was synthesized and biotinylated at the N terminus:

MLTNSSELLSKINDMPITNDQKKLMSNNVQI

For ELISA analysis of peptide-reactive serum antibodies, Nunc MediSorp plates were coated with 5 μ g/ml streptavidin (Thermo Scientific, #21122) for 1 hour at 37°C. Subsequently, ELISA plates were blocked as indicated above, followed by the addition of 2.4 μ g/ml of the biotinylated site II peptide. Coupling was performed for 1 hour at room temperature. The subsequent steps were performed as described for the antigen ELISA.

Serum competition using SPR

Approximately 300 RU of antigen was immobilized via amine coupling on a CM5 chip. Mouse sera were diluted 1:100 in HBS-EP+ running buffer and flowed as analyte with a contact time of 120 seconds to obtain an initial RU ($\text{RU}_{\text{non-blocked surface}}$). The surface was regenerated using 50 mM NaOH. Sequentially, motavizumab was injected four times at a concentration of 2 μ M, leading to complete blocking of motavizumab binding sites as confirmed by signal saturation. The same serum dilution was reinjected to determine the remaining response ($\text{RU}_{\text{blocked surface}}$). The delta serum response (SR) corresponds to the baseline-subtracted, maximum signal

of the injected sera.

$$\Delta\text{SR} = \text{RU}_{(\text{non-})\text{blocked surface}} - \text{RU}_{\text{Baseline}}$$

Percent blocking was calculated as follows:

$$\% \text{ blocking} = \left(1 - \left(\frac{\Delta\text{SR}_{\text{blocked surface}}}{\Delta\text{SR}_{\text{non-blocked surface}}} \right) \right) * 100$$

A schematic representation of the SPR experiment is shown in [S4 Fig](#), and calculated blocking values are shown in [S1 Data](#).

ELISpot

B cell ELISpot assays were performed using the Mouse IgG ELISpot HRP kit (Mabtech, #3825-2H) according to the manufacturer's instructions. Briefly, mouse spleens were isolated and pressed through a cell strainer (Corning, #352350) to obtain a single-cell suspension. Splenocytes were resuspended in RPMI media (Gibco, #11875093) supplemented with 10% FBS (Gibco), Penicillin/Streptomycin (Gibco), 0.01 $\mu\text{g/ml}$ IL2, 1 $\mu\text{g/ml}$ R848 (Mabtech, #3825-2H), and 50 μM β -mercaptoethanol (Sigma) for approximately 60 hours of stimulation at 37°C, 5% CO₂. ELISpot plates (PVDF 96-well plates, Millipore, #MSIPS4510) were coated overnight with 15 $\mu\text{g/ml}$ antigen diluted in PBS, followed by careful washing and blocking using RPMI + 10% FBS. Live splenocytes were counted, and the cell number was adjusted to 1×10^7 cells/ml. Serial dilutions of splenocytes were plated in duplicates and incubated overnight with coated plates. After several wash steps with PBS buffer, plates were incubated for 2 hours with biotinylated anti-mouse total IgG (Mabtech, #3825-6-250) in PBS, followed by incubation with streptavidin conjugated to HRP (Mabtech, #3310-9) for 1 hour. Spots were revealed using tetramethylbenzidine (TMB, Mabtech, #3651-10) and counted with an automatic reader (Bioreader 2000; BioSys GmbH). Results were represented as number of spots per 10^6 splenocytes.

RSV neutralization assay

The RSV A2 strain carrying a luciferase gene (RSV-Luc) was a kind gift of Marie-Anne Rameix-Welti, UFR des Sciences et de la Santé, Paris. Hep2 cells were seeded in Corning 96-well tissue culture plates (Sigma, #CLS3595) at a density of 40,000 cells/well in 100 μl of Minimum Essential Medium (MEM, Gibco, #11095-080) supplemented with 10% FBS (Gibco, 10500-084), L-glutamine 2 mM (Gibco, #25030-081), and penicillin-streptomycin (Gibco, #15140-122) and grown overnight at 37°C with 5% CO₂.

Sera were heat inactivated for 30 minutes at 56°C. Serial 2-fold dilutions were prepared in an untreated 96-well plate using MEM without phenol red (M0, Life Technologies, #51200-038) containing 2 mM L-glutamine, penicillin + streptomycin, and mixed with 800 pfu/well RSV-Luc (corresponding to a final MOI of 0.01). After incubating diluted sera and virus for 1 hour at 37°C, growth media were removed from the Hep2 cell layer, and 100 μl /well of the serum-virus mixture was added. After 48 hours, cells were lysed in 100 μl buffer containing 32 mM Tris (pH 7.9), 10 mM MgCl₂, 1.25% Triton X-100, 18.75% glycerol, and 1 mM DTT. Lysate (50 μl) was transferred to a 96-well plate with white background (Sigma, #CLS3912). Lysis buffer (50 μl) supplemented with 1 $\mu\text{g/ml}$ luciferin (Sigma, #L-6882) and 2 mM ATP (Sigma, #A3377) was added to each well immediately before reading luminescence signal on a Tecan Infinite 500 plate reader.

On each plate, a palivizumab dilution series was included to ensure comparability of neutralization data. In our assay, we determined IC₅₀ values for palivizumab of 0.32 $\mu\text{g/ml}$, which

is similar to what other groups have reported [41]. The neutralization curve was plotted and fitted using the GraphPad variable slope fitting model, weighted by $1/Y^2$.

Sera fractionation

Streptavidin agarose beads (400 μ l, Thermo Scientific, #20347) were pelleted at 13,000 rpm for 2 minutes in a tabletop centrifuge and washed with PBS. Biotinylated site II peptide (200 μ g) was incubated for 2 hours at room temperature to allow coupling of biotinylated peptide to streptavidin beads. Beads were washed three times with 1 ml PBS to remove excess of peptide and resuspended to a total volume of 500 μ l bead slurry. Mouse sera from the same cohort ($n = 10$) were pooled (4 μ l each, 40 μ l total) in a total volume of 200 μ l PBS, and 90 μ l diluted sera were mixed with 150 μ l of bead slurry, followed by an overnight incubation at 4°C. Beads were pelleted by centrifugation, and the supernatant was carefully removed by pipetting. Beads were then washed twice with 200 μ l PBS, and the wash fractions were discarded. To elute site II-specific antibodies, beads were resuspended in 200 μ l elution buffer (0.1 M glycine [pH 2.7]) and incubated for 1 minute before centrifugation. Supernatant was removed, neutralized with 40 μ l neutralization buffer (1 M Tris [pH 7.5], 300 mM NaCl), and stored at -20°C for subsequent testing for RSV neutralization. As a control, unconjugated streptavidin was used for each sample to account for nonspecific binding.

NGS

RNA isolation. Mouse bone marrow was isolated from femurs, resuspended in 1.5 ml Trizol (Life Technologies, #15596), and stored at -80°C until further processing. RNA extraction was performed using the PureLink RNA Mini Kit (Life Technologies, #12183018A) following the manufacturer guidelines.

Antibody sequencing library preparation. Library preparation for antibody variable heavy chain regions was performed using a protocol that incorporates unique molecular identifier (UID) tagging, as previously described by Khan and colleagues [72]. Briefly, first-strand cDNA synthesis was performed by using Maxima reverse transcriptase (Life Technologies, #EP0742) following the manufacturer instructions, using 5 μ g RNA with 20 pmol of IgG gene-specific primers (binding IgG1, IgG2a, IgG2b, IgG2c, and IgG3) with an overhang of a reverse UID (RID). After cDNA synthesis, samples were subjected to a left-hand-side SPRIselect bead (Beckman Coulter, #B23318) cleanup at 0.8X. Quantification of target-specific cDNA by a digital droplet (dd)PCR assay allowed exact input of 135,000 copies into the next PCR step. Reaction mixtures contained a forward multiplex primer set that was specific for variable heavy region framework 1 and possessed forward UID (FID), a 3' Illumina adapter specific reverse primer, and 1X KAPA HIFI HotStart Uracil+ ReadyMix (KAPA Biosystems, #KK2802). PCR reactions were then left-hand-side SPRIselect bead cleaned as before and quantified using ddPCR assay. Finally, an Illumina adaptor-extension PCR step was carried out using 820,000 copies of the previous PCR product. Following second-step adaptor-extension PCR, reactions were cleaned using a double-sided SPRIselect bead cleanup process (0.5X–0.8X) and eluted in TE buffer.

NGS with Illumina MiSeq (2 × 300 bp). After library preparation, individual NGS libraries were characterized for quality and quantified by capillary electrophoresis using a fragment analyzer (Advanced Analytical DNF-473 Standard Sensitivity). Samples were then pooled and NGS was performed on the Illumina MiSeq platform with a MiSeq Reagent Kit V3, 2 × 300 bp paired-end (Illumina, #MS-102-3003), using an input concentration of 10 pM with 10% PhiX.

Error and bias correction. Error and bias correction was performed using molecular amplification fingerprinting pipeline, as previously described [72, 73]: (1) For bioinformatic

preprocessing, paired-end FASTQ files obtained from Illumina MiSeq were imported into CLC Genomics Workbench 10 on the ETH Zurich Euler High Performance Computing (HPC) cluster. A preprocessing workflow was run containing the following steps: trimming of low-quality reads, merging of paired-end reads, removal of sequences not aligning to mouse IGH constant sequences, and length filtering. (2) For error correction by consensus building, after preprocessing all datasets were downsampled to contain the same amount of sequencing reads as the dataset with the lowest overall number of reads (361,749 sequencing reads). For error correction, a custom Python script was used to perform consensus building on the sequences, for which at least three reads per UID were required. VDJ annotation and frequency calculation was then performed by our in-house aligner [72, 73]. The complete error correction and alignment pipeline is available under <https://gitlab.ethz.ch/reddy/MAF>.

Sequence analysis and data visualization. Data analysis was done by customized scripts in R. For the identification of clonotypes, hierarchical clustering [73] was utilized to group CDR3 sequences together. The following criteria were used: identical IGHV and IGHJ gene segment usage, identical CDR3 length, and at least 80% CDR3 amino acid similarity to one other sequence in the given clonotype (single linkage). The overlap of clonotypes between both cohorts was analyzed by extracting the 20 most expanded clonotypes from each cohort and visualizing their size, occurrence, and Vgene usage by a circos plot using R software *circize* [74]. CDR3 sequence similarities between overlapping clonotypes were represented graphically with the R software *motifStack* [75]. All scripts are available upon request.

Supporting information

S1 Fig. Adjuvant screen for FFL_001 immunogen. Female Balb/c mice (five animals/group) were immunized three times (days 0, 21, 42) with 10 μ g FFL_001 monomer adsorbed to different adjuvants, and serum was analyzed on day 56. (A) Immunogenicity of FFL_001 formulated in different adjuvants. Serum titers were determined against FFL_001 at day 56 of the immunization protocol. FFL_001 adsorbed to alum showed highest overall immunogenicity. (B) Prefusion RSVF cross-reactivity of FFL_001 immunized mice after three immunizations. Four out of five mice immunized with FFL_001 formulated in alum showed serum cross-reactivity with prefusion RSVF. Data are available in [S1 Data](#). RSVF, respiratory syncytial virus fusion protein. (TIF)

S2 Fig. Homology-guided resurfacing of FFL_001. (A) Sequence alignment of FFL_001 and FFLM. (B) Resurfaced variant FFLM is monomeric in solution, as assessed by size exclusion coupled to an online multiangle-light scattering detector. Determined mass in solution is 14.7 kDa \pm 3.5%, which is close to the theoretical molecular weight of 14.4 kDa. (C) Relative surface area of RSVF antigenic site II in prefusion RSVF (PDBID 4JHW), FFLM, and NRM (model based on RSVN structure with PDBID 2WJ8). The motavizumab epitope is highlighted in red, blue patches indicate sequence changes of FFLM compared to FFL_001, and pie charts show the fraction of antigenic site II surface area compared to overall immunogen surface area. SASA was computed in PyMol in presence and absence of motavizumab. Percent SASA of antigenic site II is nearly identical when comparing RSVF and NRM, whereas the FFLM monomer shows approximately 3-fold greater relative surface area of antigenic site II, because of its small size. PDB, Protein Data Bank; RSVF, respiratory syncytial virus fusion protein; SASA, solvent accessible surface area. (TIF)

S3 Fig. SPR sensorgrams for site II nAbs. Prefusion RSVF or FFLM was immobilized on the sensor chip surface via amine coupling. Serial dilutions of site II-specific Fabs were injected as analyte. With the exception of ADII5601, which was fitted to a two-state reaction model for binding to FFLM, all data were fitted to a 1:1 Langmuir model within the Biacore evaluation software (GE Healthcare). Fab, antibody variable fragment; nAb, neutralizing antibody; RSVF, respiratory syncytial virus fusion protein; SPR, surface plasmon resonance.
(TIF)

S4 Fig. Schematic representation of the surface plasmon resonance competition assay. Mouse sera were injected on an antigen-coated sensor chip surface to measure initial response (orange). Following regeneration, motavizumab binding sites were blocked with saturating amounts of motavizumab. Residual serum response was determined on a blocked surface (blue). For data analysis, response units at indicated time points were extracted, and percent competition was calculated as described in Methods and shown in [S1 Data](#).
(TIF)

S5 Fig. Far-ultraviolet circular dichroism spectrum of antigenic site II peptide. The site II peptide adopts a flexible conformation in solution, measured in phosphate-buffered saline buffer at 25°C.
(TIF)

S6 Fig. Mice immunized with synthetic immunogen show low levels of cross-reactivity with recombinant RSVF and negligible binding to viral lysate. Mice were immunized three times with prefusion RSVF, NRM, or FFLM as shown in [Fig 2](#). (A) Sera from day 56 were analyzed by ELISA for binding to prefusion and postfusion RSVF. Prefusion RSVF-immunized mice showed lower reactivity to postfusion RSVF than to the prefusion form. FFLM- and NRM-immunized mice showed low levels of cross-reactivity with pre- and postfusion RSVF. Data shown are from one out of three independent experiments. (B) Day 56 sera from 10 mice were pooled and tested for binding to lysate of Hep2 cells, which had been infected for 48 hours with RSV. As background control, noninfected Hep2 cell lysate was prepared, and curves shown were background-subtracted. NRM-immunized mouse sera strongly react with viral lysate, whereas mice immunized with FFLM only showed negligible binding to viral lysate. The strong reactivity of NRM-immunized mice derives from antibodies raised against the RSVN carrier protein. Sera from prefusion RSVF-immunized mice are shown as control. Data shown are from one experiment performed in triplicates. Data are available in [S1 Data](#). RSVF, respiratory syncytial virus fusion protein; RSVN, RSV nucleoprotein.
(TIF)

S7 Fig. Overlapping clonotypes obtained from next-generation antibody repertoire sequencing of mice immunized with RSVF or NRM. When comparing clonotypes, defined as the same VH gene and 80% sequence similarity in the HCDR3, NRM, and RSVF immunizations yield 300 overlapping clonotypes. HCDR3, heavy chain complementarity-determining region 3; RSVF, respiratory syncytial virus fusion protein.
(TIF)

S8 Fig. Correlation of site II peptide-specific serum titer with RSV neutralization IC₅₀. Correlations for the (A) prime-only mouse cohort and the (B) homologous boost cohort. Data represent the mean of two independent experiments, each measured in duplicates. Pearson correlation coefficients (r^2) and p -values were calculated in GraphPad Prism. Data are available in [S1 Data](#). RSV, respiratory syncytial virus fusion protein.
(TIF)

S9 Fig. Enrichment of site II-specific antibodies from mouse sera. (A) Experimental setup. Streptavidin agarose beads were conjugated to biotinylated antigenic site II peptide. As control, unconjugated streptavidin beads were prepared. Sera from 10 mice within each cohort were pooled and mixed with conjugated and unconjugated beads. Column flow-through and elution fractions were analyzed by ELISA (B, C), and eluted site II-specific antibodies were analyzed in an RSV neutralization assay (D). (B) Analysis of column flow-through for site II peptide reactivity by ELISA. Immunization groups as described in Fig 4 (prime-only, homologous boost, heterologous boost, and 3x NRM). ELISA signal (OD at 450 nm) for site II peptide reactivity is shown for column flow-through from serum fractionation as depicted in (A). Streptavidin beads that were not coupled to antigenic site II peptide were used as controls and did not deplete site II reactivity in the flow-through. Data and error bars presented are averaged from two independent experiments. (C) ELISA against antigenic site II peptide of the elution fractions as shown in (A). Antibodies eluted bound specifically to the antigenic site II peptide. (D) Example RSV neutralization assay curves from elution fractions, obtained from site II conjugated (black) or unconjugated streptavidin beads (gray). Luciferase signal is plotted on the y-axis and is a measure for RSV replication as previously reported [76]. The dilution factor of purified antibodies is indicated on the x-axis. Data shown are from one experiment performed in duplicates. Data are available in [S1 Data](#). RSV, respiratory syncytial virus. (TIF)

S10 Fig. Competition ELISA with motavizumab antibody control. Plates were coated with prefusion RSVF as described in the Methods. Three-fold serial dilutions of motavizumab (initial concentration = 30 nanomolar) were prepared in presence of different competitors (RSVN, NRM, or none). Following overnight competition at 4°C, binding of motavizumab to RSVF was measured. As expected, RSVN competition did not affect RSVF binding of motavizumab. In contrast, NRM efficiently competed with RSVF for motavizumab binding at the indicated competitor concentration. Data shown are from one experiment, with error bars derived from technical duplicates. Data are available in [S1 Data](#). RSVF, respiratory syncytial virus fusion protein. (TIF)

S1 Data. Excel spreadsheet containing, in separate sheets, the underlying data for Figs 1B, 2B, 2C, 2D, 3A, 3C, 3D, 4B, 4C, 4D, 4E, 5A, 5B, 5C and 5D and S1A, S1B, S6A, S6B, S8A, S8B, S9B, S9C, S9D and S10. (XLSX)

Acknowledgments

We would like to thank the EPFL phenogenomics center (Céline Waldvogel, Raphaël Doennen) for help with the animal experiments and the protein expression core facility (David Hacker, Laurence Durrer, Soraya Quinche) for help with mammalian protein expression. We thank Davide Demurtas (CIME) and Sergey Nazarov PTBIOEM (EPFL, Lausanne, Switzerland) for electron microscopy support, as well as Nicolas Collin and Livia Brunner (Université de Lausanne) for advice on vaccine formulations. We thank Prof. Stefan Kunz (Université de Lausanne) for helpful discussions and critical reading of the manuscript.

Author Contributions

Conceptualization: Fabian Sesterhenn, Bruno E. Correia.

Data curation: Fabian Sesterhenn, Simon Friedensohn, Bruno E. Correia.

Formal analysis: Fabian Sesterhenn, Marie Galloux, Sabrina S. Vollers, Lucia Csepregi, Simon Friedensohn.

Funding acquisition: Sai T. Reddy, Bruno E. Correia.

Investigation: Fabian Sesterhenn, Marie Galloux, Sabrina S. Vollers, Lucia Csepregi, Che Yang, Delphyne Descamps, Jaume Bonet, Simon Friedensohn, Pablo Gainza, Patricia Corthésy, Man Chen, Stéphane Rosset, Marie-Anne Rameix-Welti, Bruno E. Correia.

Methodology: Fabian Sesterhenn.

Software: Simon Friedensohn.

Supervision: Jean-François Éléouët, Sai T. Reddy, Barney S. Graham, Sabine Riffault, Bruno E. Correia.

Validation: Fabian Sesterhenn.

Visualization: Fabian Sesterhenn.

Writing – original draft: Fabian Sesterhenn, Bruno E. Correia.

Writing – review & editing: Fabian Sesterhenn, Marie Galloux, Sabrina S. Vollers, Lucia Csepregi, Che Yang, Delphyne Descamps, Jaume Bonet, Simon Friedensohn, Pablo Gainza, Marie-Anne Rameix-Welti, Jean-François Éléouët, Sai T. Reddy, Barney S. Graham, Sabine Riffault, Bruno E. Correia.

References

1. Rappuoli R, Mandl CW, Black S, De Gregorio E. Vaccines for the twenty-first century society. *Nat Rev Immunol*. 2011; 11(12):865–72. <https://doi.org/10.1038/nri3085> PMID: [22051890](https://pubmed.ncbi.nlm.nih.gov/22051890/)
2. Plotkin SA. Correlates of protection induced by vaccination. *Clin Vaccine Immunol*. 2010; 17(7):1055–65. <https://doi.org/10.1128/CVI.00131-10> PMID: [20463105](https://pubmed.ncbi.nlm.nih.gov/20463105/); PubMed Central PMCID: [PMCPMC2897268](https://pubmed.ncbi.nlm.nih.gov/PMC2897268/).
3. Burton DR, Hangartner L. Broadly Neutralizing Antibodies to HIV and Their Role in Vaccine Design. *Annu Rev Immunol*. 2016; 34:635–59. <https://doi.org/10.1146/annurev-immunol-041015-055515> PMID: [27168247](https://pubmed.ncbi.nlm.nih.gov/27168247/); PubMed Central PMCID: [PMCPMC6034635](https://pubmed.ncbi.nlm.nih.gov/PMC6034635/).
4. Lee PS, Wilson IA. Structural characterization of viral epitopes recognized by broadly cross-reactive antibodies. *Curr Top Microbiol Immunol*. 2015; 386:323–41. https://doi.org/10.1007/82_2014_413 PMID: [25037260](https://pubmed.ncbi.nlm.nih.gov/25037260/); PubMed Central PMCID: [PMCPMC4358778](https://pubmed.ncbi.nlm.nih.gov/PMC6034635/).
5. Gilman MS, Castellanos CA, Chen M, Ngwuta JO, Goodwin E, Moin SM, et al. Rapid profiling of RSV antibody repertoires from the memory B cells of naturally infected adult donors. *Sci Immunol*. 2016; 1(6). <https://doi.org/10.1126/sciimmunol.aaj1879> PMID: [28111638](https://pubmed.ncbi.nlm.nih.gov/28111638/); PubMed Central PMCID: [PMCPMC5244814](https://pubmed.ncbi.nlm.nih.gov/PMC5244814/).
6. McLellan JS. Neutralizing epitopes on the respiratory syncytial virus fusion glycoprotein. *Curr Opin Virol*. 2015; 11:70–5. <https://doi.org/10.1016/j.coviro.2015.03.002> PMID: [25819327](https://pubmed.ncbi.nlm.nih.gov/25819327/); PubMed Central PMCID: [PMCPMC4456247](https://pubmed.ncbi.nlm.nih.gov/PMC4456247/).
7. Barba-Spaeth G, Dejnirattisai W, Rouvinski A, Vaney MC, Medits I, Sharma A, et al. Structural basis of potent Zika-dengue virus antibody cross-neutralization. *Nature*. 2016; 536(7614):48–53. <https://doi.org/10.1038/nature18938> PMID: [27338953](https://pubmed.ncbi.nlm.nih.gov/27338953/).
8. Robbiani DF, Bozzacco L, Keeffe JR, Khouri R, Olsen PC, Gazumyan A, et al. Recurrent Potent Human Neutralizing Antibodies to Zika Virus in Brazil and Mexico. *Cell*. 2017; 169(4):597–609 e11. <https://doi.org/10.1016/j.cell.2017.04.024> PMID: [28475892](https://pubmed.ncbi.nlm.nih.gov/28475892/); PubMed Central PMCID: [PMCPMC5492969](https://pubmed.ncbi.nlm.nih.gov/PMC5492969/).
9. Xu M, Zuest R, Velumani S, Tukijan F, Toh YX, Appanna R, et al. A potent neutralizing antibody with therapeutic potential against all four serotypes of dengue virus. *NPJ Vaccines*. 2017; 2:2. <https://doi.org/10.1038/s41541-016-0003-3> PMID: [29263863](https://pubmed.ncbi.nlm.nih.gov/29263863/); PubMed Central PMCID: [PMCPMC5627287](https://pubmed.ncbi.nlm.nih.gov/PMC5627287/).
10. Bornholdt ZA, Turner HL, Murin CD, Li W, Sok D, Souders CA, et al. Isolation of potent neutralizing antibodies from a survivor of the 2014 Ebola virus outbreak. *Science*. 2016; 351(6277):1078–83. <https://doi.org/10.1126/science.aad5788> PMID: [26912366](https://pubmed.ncbi.nlm.nih.gov/26912366/); PubMed Central PMCID: [PMCPMC4900763](https://pubmed.ncbi.nlm.nih.gov/PMC4900763/).

11. Chandramouli S, Malito E, Nguyen T, Luisi K, Donnarumma D, Xing Y, et al. Structural basis for potent antibody-mediated neutralization of human cytomegalovirus. *Sci Immunol*. 2017; 2(12). <https://doi.org/10.1126/sciimmunol.aan1457> PMID: 28783665.
12. Hastie KM, Zandonatti MA, Kleinfelter LM, Heinrich ML, Rowland MM, Chandran K, et al. Structural basis for antibody-mediated neutralization of Lassa virus. *Science*. 2017; 356(6341):923–8. <https://doi.org/10.1126/science.aam7260> PMID: 28572385; PubMed Central PMCID: PMC6007842.
13. Harrison SC. Viral membrane fusion. *Virology*. 2015; 479–480:498–507. <https://doi.org/10.1016/j.virol.2015.03.043> PMID: 25866377; PubMed Central PMCID: PMC604424100.
14. Corti D, Voss J, Gamblin SJ, Codoni G, Macagno A, Jarrossay D, et al. A neutralizing antibody selected from plasma cells that binds to group 1 and group 2 influenza A hemagglutinins. *Science*. 2011; 333(6044):850–6. <https://doi.org/10.1126/science.1205669> PMID: 21798894.
15. McLellan JS, Chen M, Leung S, Graepel KW, Du X, Yang Y, et al. Structure of RSV fusion glycoprotein trimer bound to a prefusion-specific neutralizing antibody. *Science*. 2013; 340(6136):1113–7. <https://doi.org/10.1126/science.1234914> PMID: 23618766; PubMed Central PMCID: PMC604459498.
16. Burton DR. Antibodies, viruses and vaccines. *Nat Rev Immunol*. 2002; 2(9):706–13. <https://doi.org/10.1038/nri891> PMID: 12209139.
17. Burton DR. What Are the Most Powerful Immunogen Design Vaccine Strategies? Reverse Vaccinology 2.0 Shows Great Promise. *Cold Spring Harb Perspect Biol*. 2017; 9(11). <https://doi.org/10.1101/cshperspect.a030262> PMID: 28159875; PubMed Central PMCID: PMC605540812.
18. Rappuoli R, Bottomley MJ, D'Oro U, Finco O, De Gregorio E. Reverse vaccinology 2.0: Human immunology instructs vaccine antigen design. *J Exp Med*. 2016; 213(4):469–81. <https://doi.org/10.1084/jem.20151960> PMID: 27022144; PubMed Central PMCID: PMC604821650.
19. McLellan JS, Chen M, Joyce MG, Sastry M, Stewart-Jones GB, Yang Y, et al. Structure-based design of a fusion glycoprotein vaccine for respiratory syncytial virus. *Science*. 2013; 342(6158):592–8. <https://doi.org/10.1126/science.1243283> PMID: 24179220; PubMed Central PMCID: PMC604461862.
20. Impagliazzo A, Milder F, Kuipers H, Wagner MV, Zhu X, Hoffman RM, et al. A stable trimeric influenza hemagglutinin stem as a broadly protective immunogen. *Science*. 2015; 349(6254):1301–6. <https://doi.org/10.1126/science.aac7263> PMID: 26303961.
21. Yassine HM, Boyington JC, McTamney PM, Wei CJ, Kanekiyo M, Kong WP, et al. Hemagglutinin-stem nanoparticles generate heterosubtypic influenza protection. *Nat Med*. 2015; 21(9):1065–70. <https://doi.org/10.1038/nm.3927> PMID: 26301691.
22. Correia BE, Bates JT, Loomis RJ, Baneyx G, Carrico C, Jardine JG, et al. Proof of principle for epitope-focused vaccine design. *Nature*. 2014; 507(7491):201–6. <https://doi.org/10.1038/nature12966> PMID: 24499818; PubMed Central PMCID: PMC604260937.
23. Finlay BB, McFadden G. Anti-immunology: evasion of the host immune system by bacterial and viral pathogens. *Cell*. 2006; 124(4):767–82. <https://doi.org/10.1016/j.cell.2006.01.034> PMID: 16497587.
24. Andrews SF, Huang Y, Kaur K, Popova LI, Ho IY, Pauli NT, et al. Immune history profoundly affects broadly protective B cell responses to influenza. *Sci Transl Med*. 2015; 7(316):316ra192. <https://doi.org/10.1126/scitranslmed.aad0522> PMID: 26631631; PubMed Central PMCID: PMC604770855.
25. Angeletti D, Gibbs JS, Angel M, Kosik I, Hickman HD, Frank GM, et al. Defining B cell immunodominance to viruses. *Nat Immunol*. 2017; 18(4):456–63. <https://doi.org/10.1038/ni.3680> PMID: 28192417; PubMed Central PMCID: PMC605360521.
26. Zarnitsyna VI, Ellebedy AH, Davis C, Jacob J, Ahmed R, Antia R. Masking of antigenic epitopes by antibodies shapes the humoral immune response to influenza. *Philos Trans R Soc Lond B Biol Sci*. 2015; 370(1676). <https://doi.org/10.1098/rstb.2014.0248> PMID: 26194761; PubMed Central PMCID: PMC604528424.
27. Zarnitsyna VI, Lavine J, Ellebedy A, Ahmed R, Antia R. Multi-epitope Models Explain How Pre-existing Antibodies Affect the Generation of Broadly Protective Responses to Influenza. *PLoS Pathog*. 2016; 12(6):e1005692. <https://doi.org/10.1371/journal.ppat.1005692> PMID: 27336297; PubMed Central PMCID: PMC604918916.
28. Victora GD, Nussenzweig MC. Germinal centers. *Annu Rev Immunol*. 2012; 30:429–57. <https://doi.org/10.1146/annurev-immunol-020711-075032> PMID: 22224772.
29. Briney B, Sok D, Jardine JG, Kulp DW, Skog P, Menis S, et al. Tailored Immunogens Direct Affinity Maturation toward HIV Neutralizing Antibodies. *Cell*. 2016; 166(6):1459–70 e11. <https://doi.org/10.1016/j.cell.2016.08.005> PMID: 27610570; PubMed Central PMCID: PMC605018249.
30. Jardine JG, Ota T, Sok D, Pauthner M, Kulp DW, Kalyuzhnyi O, et al. HIV-1 VACCINES. Priming a broadly neutralizing antibody response to HIV-1 using a germline-targeting immunogen. *Science*. 2015; 349(6244):156–61. <https://doi.org/10.1126/science.aac5894> PMID: 26089355; PubMed Central PMCID: PMC604669217.

31. Silva M, Nguyen TH, Philbrook P, Chu M, Sears O, Hatfield S, et al. Targeted Elimination of Immunodominant B Cells Drives the Germinal Center Reaction toward Subdominant Epitopes. *Cell Rep.* 2017; 21(13):3672–80. <https://doi.org/10.1016/j.celrep.2017.12.014> PMID: 29281817; PubMed Central PMCID: PMC5771444.
32. Boyington JC, Joyce MG, Sastry M, Stewart-Jones GB, Chen M, Kong WP, et al. Structure-Based Design of Head-Only Fusion Glycoprotein Immunogens for Respiratory Syncytial Virus. *PLoS ONE.* 2016; 11(7):e0159709. <https://doi.org/10.1371/journal.pone.0159709> PMID: 27463224; PubMed Central PMCID: PMC4963090.
33. Kirchenbaum GA, Carter DM, Ross TM. Sequential Infection in Ferrets with Antigenically Distinct Seasonal H1N1 Influenza Viruses Boosts Hemagglutinin Stalk-Specific Antibodies. *J Virol.* 2016; 90(2):1116–28. <https://doi.org/10.1128/JVI.02372-15> PMID: 26559834; PubMed Central PMCID: PMC4702689.
34. Van Reeth K, Gracia JCM, Trus I, Sys L, Claes G, Versnaeyen H, et al. Heterologous prime-boost vaccination with H3N2 influenza viruses of swine favors cross-clade antibody responses and protection. *NPJ Vaccines.* 2017; 2. <https://doi.org/10.1038/s41541-017-0012-x> PMID: 29250437; PubMed Central PMCID: PMC5604745.
35. Wei CJ, Boyington JC, McTamney PM, Kong WP, Pearce MB, Xu L, et al. Induction of broadly neutralizing H1N1 influenza antibodies by vaccination. *Science.* 2010; 329(5995):1060–4. <https://doi.org/10.1126/science.1192517> PMID: 20647428
36. Herve PL, Deloizy C, Descamps D, Rameix-Welti MA, Fix J, McLellan JS, et al. RSV N-nanorings fused to palivizumab-targeted neutralizing epitope as a nanoparticle RSV vaccine. *Nanomedicine.* 2017; 13(2):411–20. <https://doi.org/10.1016/j.nano.2016.08.006> PMID: 27553073.
37. Roux X, Dubuquoy C, Durand G, Tran-Tolla TL, Castagne N, Bernard J, et al. Sub-nucleocapsid nanoparticles: a nasal vaccine against respiratory syncytial virus. *PLoS ONE.* 2008; 3(3):e1766. <https://doi.org/10.1371/journal.pone.0001766> PMID: 18335041; PubMed Central PMCID: PMC2262139.
38. Tawar RG, Duquerroy S, Vonrhein C, Varela PF, Damier-Piolle L, Castagne N, et al. Crystal structure of a nucleocapsid-like nucleoprotein-RNA complex of respiratory syncytial virus. *Science.* 2009; 326(5957):1279–83. <https://doi.org/10.1126/science.1177634> PMID: 19965480.
39. Correia BE, Ban YE, Friend DJ, Ellingson K, Xu H, Boni E, et al. Computational protein design using flexible backbone remodeling and resurfacing: case studies in structure-based antigen design. *J Mol Biol.* 2011; 405(1):284–97. <https://doi.org/10.1016/j.jmb.2010.09.061> PMID: 20969873.
40. Kuhlman B, Baker D. Native protein sequences are close to optimal for their structures. *Proc Natl Acad Sci U S A.* 2000; 97(19):10383–8. PMID: 10984534; PubMed Central PMCID: PMC27033.
41. Wu H, Pfarr DS, Johnson S, Brewah YA, Woods RM, Patel NK, et al. Development of motavizumab, an ultra-potent antibody for the prevention of respiratory syncytial virus infection in the upper and lower respiratory tract. *J Mol Biol.* 2007; 368(3):652–65. <https://doi.org/10.1016/j.jmb.2007.02.024> PMID: 17362988.
42. Joyce MG, Zhang B, Ou L, Chen M, Chuang GY, Druz A, et al. Iterative structure-based improvement of a fusion-glycoprotein vaccine against RSV. *Nat Struct Mol Biol.* 2016; 23(9):811–20. <https://doi.org/10.1038/nsmb.3267> PMID: 27478931; PubMed Central PMCID: PMC5016229.
43. McLellan JS, Correia BE, Chen M, Yang Y, Graham BS, Schief WR, et al. Design and characterization of epitope-scaffold immunogens that present the motavizumab epitope from respiratory syncytial virus. *J Mol Biol.* 2011; 409(5):853–66. <https://doi.org/10.1016/j.jmb.2011.04.044> PMID: 21549714; PubMed Central PMCID: PMC3107930.
44. McLellan JS, Chen M, Kim A, Yang Y, Graham BS, Kwong PD. Structural basis of respiratory syncytial virus neutralization by motavizumab. *Nat Struct Mol Biol.* 2010; 17(2):248–50. <https://doi.org/10.1038/nsmb.1723> PMID: 20098425; PubMed Central PMCID: PMC3050594.
45. Xu JL, Davis MM. Diversity in the CDR3 region of V(H) is sufficient for most antibody specificities. *Immunity.* 2000; 13(1):37–45. PMID: 10933393.
46. Scheid JF, Mouquet H, Ueberheide B, Diskin R, Klein F, Oliveira TY, et al. Sequence and structural convergence of broad and potent HIV antibodies that mimic CD4 binding. *Science.* 2011; 333(6049):1633–7. <https://doi.org/10.1126/science.1207227> PMID: 21764753; PubMed Central PMCID: PMC3351836.
47. Goodwin E, Gilman MSA, Wrapp D, Chen M, Ngwuta JO, Moin SM, et al. Infants Infected with Respiratory Syncytial Virus Generate Potent Neutralizing Antibodies that Lack Somatic Hypermutation. *Immunity.* 2018; 48(2):339–49 e5. <https://doi.org/10.1016/j.immuni.2018.01.005> PMID: 29396163; PubMed Central PMCID: PMC6005179.
48. Friedensohn S, Khan TA, Reddy ST. Advanced Methodologies in High-Throughput Sequencing of Immune Repertoires. *Trends Biotechnol.* 2017; 35(3):203–14. <https://doi.org/10.1016/j.tibtech.2016.09.010> PMID: 28341036.

49. Kallewaard NL, Corti D, Collins PJ, Neu U, McAuliffe JM, Benjamin E, et al. Structure and Function Analysis of an Antibody Recognizing All Influenza A Subtypes. *Cell*. 2016; 166(3):596–608. <https://doi.org/10.1016/j.cell.2016.05.073> PMID: 27453466; PubMed Central PMCID: PMC4967455.
50. Sesterhenn F, Bonet J, Correia BE. Structure-based immunogen design-leading the way to the new age of precision vaccines. *Curr Opin Struct Biol*. 2018; 51:163–9. <https://doi.org/10.1016/j.sbi.2018.06.002> PMID: 29980105.
51. Ofek G, Guenaga FJ, Schief WR, Skinner J, Baker D, Wyatt R, et al. Elicitation of structure-specific antibodies by epitope scaffolds. *Proc Natl Acad Sci U S A*. 2010; 107(42):17880–7. <https://doi.org/10.1073/pnas.1004728107> PMID: 20876137; PubMed Central PMCID: PMC2964213.
52. Jaberolansar N, Chappell KJ, Watterson D, Bermingham IM, Toth I, Young PR, et al. Induction of high titred, non-neutralising antibodies by self-adjuvanting peptide epitopes derived from the respiratory syncytial virus fusion protein. *Sci Rep*. 2017; 7(1):11130. <https://doi.org/10.1038/s41598-017-10415-w> PMID: 28894111; PubMed Central PMCID: PMC5593926.
53. Abbott RK, Lee JH, Menis S, Skog P, Rossi M, Ota T, et al. Precursor Frequency and Affinity Determine B Cell Competitive Fitness in Germinal Centers, Tested with Germline-Targeting HIV Vaccine Immunogens. *Immunity*. 2018; 48(1):133–46 e6. <https://doi.org/10.1016/j.immuni.2017.11.023> PMID: 29287996; PubMed Central PMCID: PMC5773359.
54. Correia BE, Ban YE, Holmes MA, Xu H, Ellingson K, Kraft Z, et al. Computational design of epitope-scaffolds allows induction of antibodies specific for a poorly immunogenic HIV vaccine epitope. *Structure*. 2010; 18(9):1116–26. <https://doi.org/10.1016/j.str.2010.06.010> PMID: 20826338.
55. Victora GD, Wilson PC. Germinal Center Selection and the Antibody Response to Influenza. *Cell*. 2015; 163(3):545–8. <https://doi.org/10.1016/j.cell.2015.10.004> PubMed PMID: WOS:000364828900009. PMID: 26496601
56. Tsui P, Tornetta MA, Ames RS, Bankosky BC, Griego S, Silverman C, et al. Isolation of a neutralizing human RSV antibody from a dominant, non-neutralizing immune repertoire by epitope-blocked panning. *Journal of Immunology*. 1996; 157(2):772–80. PubMed PMID: WOS:A1996UW15400036.
57. Widjaja I, Wicht O, Luytjes W, Leenhouts K, Rottier PJM, van Kuppeveld FJM, et al. Characterization of Epitope-Specific Anti-Respiratory Syncytial Virus (Anti-RSV) Antibody Responses after Natural Infection and after Vaccination with Formalin-Inactivated RSV. *J Virol*. 2016; 90(13):5965–77. <https://doi.org/10.1128/JVI.00235-16> PMID: 27099320; PubMed Central PMCID: PMC4907225.
58. Andrews SF, Kaur K, Pauli NT, Huang M, Huang Y, Wilson PC. High preexisting serological antibody levels correlate with diversification of the influenza vaccine response. *J Virol*. 2015; 89(6):3308–17. <https://doi.org/10.1128/JVI.02871-14> PMID: 25589639; PubMed Central PMCID: PMC4337521.
59. Xu K, Acharya P, Kong R, Cheng C, Chuang GY, Liu K, et al. Epitope-based vaccine design yields fusion peptide-directed antibodies that neutralize diverse strains of HIV-1. *Nat Med*. 2018; 24(6):857–67. <https://doi.org/10.1038/s41591-018-0042-6> PMID: 29867235.
60. Li Y, Myers JL, Bostick DL, Sullivan CB, Madara J, Linderman SL, et al. Immune history shapes specificity of pandemic H1N1 influenza antibody responses. *J Exp Med*. 2013; 210(8):1493–500. <https://doi.org/10.1084/jem.20130212> PMID: 23857983; PubMed Central PMCID: PMC3727314.
61. Ekiert DC, Friesen RH, Bhabha G, Kwaks T, Jongeneelen M, Yu W, et al. A highly conserved neutralizing epitope on group 2 influenza A viruses. *Science*. 2011; 333(6044):843–50. <https://doi.org/10.1126/science.1204839> PMID: 21737702; PubMed Central PMCID: PMC3210727.
62. Raymond DD, Bajic G, Ferdman J, Suphaphiphat P, Settembre EC, Moody MA, et al. Conserved epitope on influenza-virus hemagglutinin head defined by a vaccine-induced antibody. *Proc Natl Acad Sci U S A*. 2018; 115(1):168–73. <https://doi.org/10.1073/pnas.1715471115> PMID: 29255041; PubMed Central PMCID: PMC5776812.
63. Dejnirattisai W, Supasa P, Wongwiwat W, Rouvinski A, Barba-Spaeth G, Duangchinda T, et al. Dengue virus sero-cross-reactivity drives antibody-dependent enhancement of infection with zika virus. *Nat Immunol*. 2016; 17(9):1102–8. <https://doi.org/10.1038/ni.3515> PMID: 27339099; PubMed Central PMCID: PMC4994874.
64. Katzelnick LC, Gresh L, Halloran ME, Mercado JC, Kuan G, Gordon A, et al. Antibody-dependent enhancement of severe dengue disease in humans. *Science*. 2017; 358(6365):929–32. <https://doi.org/10.1126/science.aan6836> PMID: 29097492; PubMed Central PMCID: PMC5858873.
65. Bonet J, Wehrle S, Schriever K, Yang C, Billet A, Sesterhenn F, et al. Rosetta FunFolDes—A general framework for the computational design of functional proteins. *PLoS Comput Biol*. 2018; 14(11): e1006623. <https://doi.org/10.1371/journal.pcbi.1006623> PMID: 30452434; PubMed Central PMCID: PMC6277116.
66. Sievers F, Wilm A, Dineen D, Gibson TJ, Karplus K, Li W, et al. Fast, scalable generation of high-quality protein multiple sequence alignments using Clustal Omega. *Mol Syst Biol*. 2011; 7:539. <https://doi.org/10.1038/msb.2011.75> PMID: 21988835; PubMed Central PMCID: PMC3261699.

67. Castagne N, Barbier A, Bernard J, Rezaei H, Huet JC, Henry C, et al. Biochemical characterization of the respiratory syncytial virus P-P and P-N protein complexes and localization of the P protein oligomerization domain. *J Gen Virol*. 2004; 85(Pt 6):1643–53. <https://doi.org/10.1099/vir.0.79830-0> PMID: 15166449.
68. Rohou A, Grigorieff N. CTFIND4: Fast and accurate defocus estimation from electron micrographs. *J Struct Biol*. 2015; 192(2):216–21. <https://doi.org/10.1016/j.jsb.2015.08.008> PMID: 26278980.
69. de la Rosa-Trevin JM, Quintana A, Del Cano L, Zaldivar A, Foche I, Gutierrez J, et al. Scipion: A software framework toward integration, reproducibility and validation in 3D electron microscopy. *J Struct Biol*. 2016; 195(1):93–9. <https://doi.org/10.1016/j.jsb.2016.04.010> PMID: 27108186.
70. Scheres SH. RELION: implementation of a Bayesian approach to cryo-EM structure determination. *J Struct Biol*. 2012; 180(3):519–30. <https://doi.org/10.1016/j.jsb.2012.09.006> PMID: 23000701; PubMed Central PMCID: PMC3690530.
71. Kulp DW, Steichen JM, Pauthner M, Hu X, Schiffner T, Liguori A, et al. Structure-based design of native-like HIV-1 envelope trimers to silence non-neutralizing epitopes and eliminate CD4 binding. *Nat Commun*. 2017; 8(1):1655. <https://doi.org/10.1038/s41467-017-01549-6> PMID: 29162799; PubMed Central PMCID: PMC5698488.
72. Khan TA, Friedensohn S, Gorter de Vries AR, Straszewski J, Ruscheweyh HJ, Reddy ST. Accurate and predictive antibody repertoire profiling by molecular amplification fingerprinting. *Sci Adv*. 2016; 2(3): e1501371. <https://doi.org/10.1126/sciadv.1501371> PMID: 26998518; PubMed Central PMCID: PMC4795664.
73. Friedensohn S, Lindner JM, Cornacchione V, Iazeolla M, Miho E, Zingg A, et al. Synthetic Standards Combined With Error and Bias Correction Improve the Accuracy and Quantitative Resolution of Antibody Repertoire Sequencing in Human Naive and Memory B Cells. *Front Immunol*. 2018; 9:1401. <https://doi.org/10.3389/fimmu.2018.01401> PMID: 29973938; PubMed Central PMCID: PMC6019461.
74. Gu Z, Gu L, Eils R, Schlesner M, Brors B. circlize Implements and enhances circular visualization in R. *Bioinformatics*. 2014; 30(19):2811–2. <https://doi.org/10.1093/bioinformatics/btu393> PMID: 24930139
75. Ou J, Wolfe SA, Brodsky MH, Zhu LJ. motifStack for the analysis of transcription factor binding site evolution. *Nat Methods*. 2018; 15(1):8–9. <https://doi.org/10.1038/nmeth.4555> PMID: 29298290.
76. Rameix-Welti MA, Le Goffic R, Herve PL, Sourimant J, Remot A, Riffault S, et al. Visualizing the replication of respiratory syncytial virus in cells and in living mice. *Nat Commun*. 2014; 5:5104. <https://doi.org/10.1038/ncomms6104> PMID: 25277263.